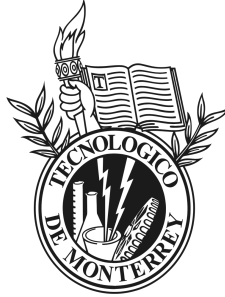


Instituto Tecnológico y de Estudios Superiores de Monterrey
Campus Monterrey
School of Engineering and Sciences



Development of a wirelessly-controlled electrolysis
pump for automation of bioanalytical assays in
Centrifugal Microfluidic Devices

A thesis presented by:

Fabian Oswaldo Romero Soto

Submitted to the School of Engineering and Sciences
in partial fulfillment of the requirements for the degree of

Master on Nanotechnology

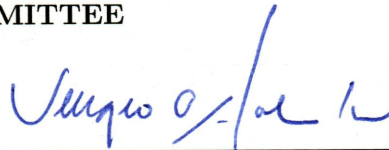
Monterrey, N.L.

December, 2019

**Instituto Tecnológico y de Estudios Superiores de Monterrey
Campus Monterrey
School of Engineering and Sciences**

The committee members, hereby, certify that have read the thesis presented by Fabian Oswaldo Romero Soto and that it is fully adequate in scope and quality as a partial requirement for the degree of *Master on Nanotechnology*.

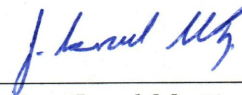
THESIS COMMITTEE



Sergio Omar Martinez Chapa, PhD
Instituto Tecnológico y de Estudios Superiores de Monterrey
School of Engineering and Sciences
Monterrey, N.L.
Principal Adviser



Mohammad Mahdi Aeinehvand, PhD
Instituto Tecnológico y de Estudios Superiores de Monterrey
School of Engineering and Sciences
Monterrey, N.L.
Co-Adviser



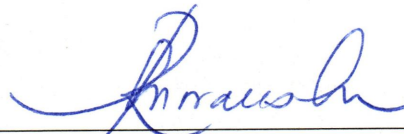
Jose Israel Martinez Lopez, PhD
Instituto Tecnológico y de Estudios Superiores de Monterrey
School of Engineering and Sciences
Monterrey, N.L.
Committee Member



**Tecnológico
de Monterrey**

19 NOV 2019

Dirección Nacional de Posgrado
Dr. Rubén Morales Menéndez



Ruben Morales Menendez, PhD
Dean of Graduate Studies
School of Engineering and Sciences

Monterrey, N.L., December, 2019

Declaration of Authorship

I, Fabian Oswaldo Romero Soto declare that this thesis titled, Development of a wirelessly-controlled electrolysis pump for automation of bioanalytical assays in Centrifugal Microfluidic Devices and the work presented in it are my own. I confirm that:

- This work was done wholly or mainly while in candidature for a research degree at this University.
- Where any part of this thesis has previously been submitted for a degree or any other qualification at this University or any other institution, this has been clearly stated.
- Where I have consulted the published work of others, this is always clearly attributed.
- Where I have quoted from the work of others, the source is always given. With the exception of such quotations, this thesis is entirely my own work.
- I have acknowledged all main sources of help.
- Where the thesis is based on work done by myself jointly with others, I have made clear exactly what was done by others and what I have contributed myself.



FABIAN OSWALDO ROMERO SOTO
Monterrey, N.L., December, 2019

Dedicatory

I would like to dedicate this work to my parents, Vicente and Evelyn, by all the help, love and trust they gave me during all my academic trajectory; to my brother Francisco and my sisters Vivian and Lilian, for a lot of good moments when we are together; To my grandparents Alejandra, Vicente, Nelly and Osvaldo, by all the support and time when I needed it; To Carolina, for her trust and encouragement in the last stages of the project.

Acknowledgments

I would like to express my gratitude to all those persons that made possible to get this project in final stages. To my principal adviser, Sergio Omar Martinez Chapa, by giving me the opportunity to begin my researcher path with this project and his incredible advices during these years. To my co-adviser and dear friend, Mohammad Mahdi Aeinehvand, for his patience and guidance to work smoothly in research and microfluidics. Both, Dr. Sergio and Dr. Mohammad, supported me with the resources and teaching to develop this work. To my dear friends, M.C. Martin Francisco Jimenez Moreno and Eng. Mauricio Binny Jind, by giving me their advices, knowledge and fun moments during my Master studies. To Dr. Jose Israel Martinez Lopez and Dr. Roberto Carlos Gallo Villanueva, by giving their time and guidance during the final stages of my thesis. To Dr. Dario Mager's group, for providing me the equipment and help during my stay on Germany to run the final assays and to the Dr. Laura Weber, by teaching me and aiding me during the last days to test the immunoassays. Sincerely, thank you to all the people that were and are with me and their trust.

I am grateful to CONACYT for giving me the support during these years (CVU 885739), making me discover and develop my potential as researcher. I am grateful to the Tecnológico de Monterrey for giving me the possibility to continue my studies in the master level, as well as for providing their installations and resources during my thesis. This thesis work has been supported by the CONACYT grant no. 267726: "Development of a CD-Based Microfluidic Platform with Electrochemical and Optical Sensing for Medical Diagnostics and Environmental Monitoring", of the 2015 CONACYT-DAAD Program.

FABIAN OSWALDO ROMERO SOTO

Instituto Tecnológico y de Estudios Superiores de Monterrey, December, 2019

Abstract

Development of a wirelessly-controlled electrolysis pump for automation of bioanalytical assays in Centrifugal Microfluidic Devices

Bioanalytical assays for diagnosis of infectious diseases are typically performed in sophisticated labs with highly trained technicians. Unfortunately, these labs are not accessible to everybody because the service is either expensive or far from the patients in unprivileged and remote areas. Reaching millions of people, particularly in the rural environment of developing countries needs more affordable technologies. Centrifugal Microfluidic Devices have been used to automate complex bioanalytical assays and the technology has reached good maturity. However, incorporation of other techniques to manipulate the fluid, aside from the centrifugal forces, will increase the applicability of the technology for “Point-of-Care” diagnosis. Particularly, the availability of small-footprint pumps able to supply specific amounts of fluid during the different assay steps will allow integration of much more complex assays in a single disc. Conveniently, recent electrification of centrifugal microfluidic devices has opened the possibility to incorporate electrical and electrochemical sensors and actuators to the discs, which can even be controlled wirelessly. This work presents the design and implementation of a wirelessly-controlled electrolysis pump for centrifugal microfluidics platforms. By applying an electrical current to water in a chamber, electrolysis and subsequent accumulation of gases create a pneumatic pressure that enables the supply of specific fluid volumes during the different stages of complex assays. As a proof of concept, a centrifugal microfluidic device with a series of electrolysis pumps has been developed to automate a peptides-microarray-based immunoassay for the detection of influenza Hemagglutinin (HA) proteins.

Fabian Oswaldo Romero Soto

List of Figures

1.1	Budget percentage destined to health care some American countries in 2016	2
2.1	Electrolysis pump based on membrane deflection	6
2.2	Examples of microfluidic devices using electrolysis pump for biological applications	7
3.1	Pseudo-forces in LoaD platforms	12
3.2	Schematic illustration of mechanism of the RTPV	14
3.3	Schematic illustration of basic water electrolysis	16
3.4	Electrical circuit analogy for resistances presented in water electrolysis	17
3.5	Schematic illustration of electrolysis pump	18
3.6	Schematic illustration of the electrolysis pumping process	19
3.7	Illustration highlighting parameters for the electrolysis pump	20
3.8	Descriptive layout of the eLoaD platform	22
3.9	Biotin patterns as examples of peptides microarrays analyzed by fluorescence	24
3.10	Schematic of a typical peptides microarray experiment	25
3.11	The growth of peptides on array format by using particle-based synthesis	26
4.1	Thesis flowchart represented in block diagram	28
4.2	The actuation of the remodeled miniaturized electrolysis.	29
4.3	Schematic illustration of top view of the Schematic of the Reversible Thermo-Pneumatic Valve	30
4.4	Design and layers of the CD developed for the characterization of the wireless electrolysis pump and the automation of immunoassay	33
4.5	Photos of CDs used for Phase 1 and Phase 2.	34
4.6	Block diagrams about the general operation of the android application and eLoaD circuit	35
4.7	The mobile application developed for wireless control of electrolysis pumps and RTPV valves	36
4.8	Photos and illustration of the PCB board used during the work	38
4.9	Pyrolysis protocol used for GC electrodes/Photos of pyrolyzed GC electrodes	40
4.10	Experimental setup for the multiple studying CD platforms developed in this work	41
4.11	Schematic illustration of the performance of Phase 4 CD in an immunoassay	43

5.1	Pneumatic pressure required to move liquid volume by electrolysis pump at different rotational speeds	45
5.2	Experimental and theoretical analysis of carbon electrolysis pumping flow rate while increasing the rotational speed.	46
5.3	Experimental and theoretical analysis of electrolysis pumping flow rate at different electrical current.	48
5.4	Fluorescence scans of control and CD peptides microarrays and their average intensities	49
7.1	LTSpice simulation about the current output using OP777	61
7.2	Circuit diagram of the PCB board used for immunoassay test (Phase 2 CD)	62
7.3	First CD design for adaptation of the immunoassay protocol	63
7.4	Photos showing the operation of the initial CD design	64
7.5	Screenshot of block programming for android application used on Phase 2 CD	65

List of Tables

1.1	1.1 Number of cases of sickness by infection reported by the Mexican Ministry of Health in 2014 and 2018.	1
2.1	Summary of microfluidic devices where the electrolysis pump was implemented.	8
3.1	Properties of commercial glassy carbon electrodes.	22
3.2	Power management of the eLoaD disc for centrifugal microfluidic applications.	23
4.1	Parameters used to design and model the electrolysis pump. . .	31

Contents

Abstract	iv
List of Figures	vi
List of Tables	vii
1 Introduction	1
2 State of Art	5
2.1 Electrolysis pump on microfluidic Chips	5
2.2 Automation of Immunoassay on Lab on a Disc	9
3 Background	11
3.1 Lab on a Disc	11
3.2 Unit operation: Active valves and RTPV valve	13
3.3 Electrolysis of water: Theory	16
3.4 Unit operation: Electrolysis pump	17
3.5 Glassy carbon electrodes	21
3.6 electrified Lab on a Disc (eLoaD)	22
3.7 Peptides Microarrays	24
4 Materials and methods	27
4.1 Unit operations design: Electrolysis pump and RTPV	29
4.2 CD designs and fabrication	30
4.3 eLoaD implementation: electrical circuit and mobile application design .	34
4.4 Glassy carbon electrodes fabrication	39
4.5 Experimental setup and procedure	39
5 Results and Discussion	44
5.1 Flow rate characterization during pumping regime	44
5.2 Peptides microarray protocol on CD platform	48
6 Conclusions and future work	50
6.1 Conclusions	50
6.2 Future work	51
7 Bibliography	52

Appendix A	61
Appendix B	65

Chapter 1

Introduction

The last influenza pandemic (2009 H1N1 crisis) has highlighted the challenges that the government and clinical facilities must face to reduce in the impact of high-scale infections, especially in surveillance network. Little attention has been given to early detection after the improved regulation, and only a few studies were found [1]. Galindo-Fraga et al. studied the tendency to get respiratory infection such as Influenza and illness-like- influenza in five hospitals in Mexico city. In the period of 2010-2011, 1065 cases were documented among which 54.9% required hospitalization and 6.6% died by the infection [2].

In recent years, Mexico has not improved the regulations and methods for early detection of infectious diseases. In 2014, the Ministry of Health reported the number of patients with infectious diseases related to the respiratory, digestive and urinary systems as (27,493,239), (4,941,427) and (4,244,053) cases respectively [3]. In the last year, the main causes of morbidity did not change neither the number of causes of each infection demonstrating that there has not been improvement for early detection and prevention in Mexico [4]. **Table 1.1** compares the number of cases documented in the years 2014 and 2018.

Type of infection	Number of cases in 2014	Number of cases in 2018
Respiratory	27,493,239	24,462,860
Digestive	4,941,427	5,375,702
Urinary	4,244,053	4 339 674

Table 1.1: **1.1 Number of cases of sickness by infection reported by the Mexican Ministry of Health in 2014 and 2018.**

The poor performance of Mexico for infection control can be derived by the low budget used in healthcare. **Figure 1.1** shows a bars graph comparing the percentage dedicated to health expenses in some countries in America during 2016 [5]. The budget in Mexico was low in comparison with neighboring countries such as the United States, Canada and Guatemala. The lack of consumables and diagnostic equipment in overpopulated areas in Mexico is a reflection of this situation. The previous statement remarks the need to search alternative equipment able of accomplishing the demand for diagnosis with the current circumstances.

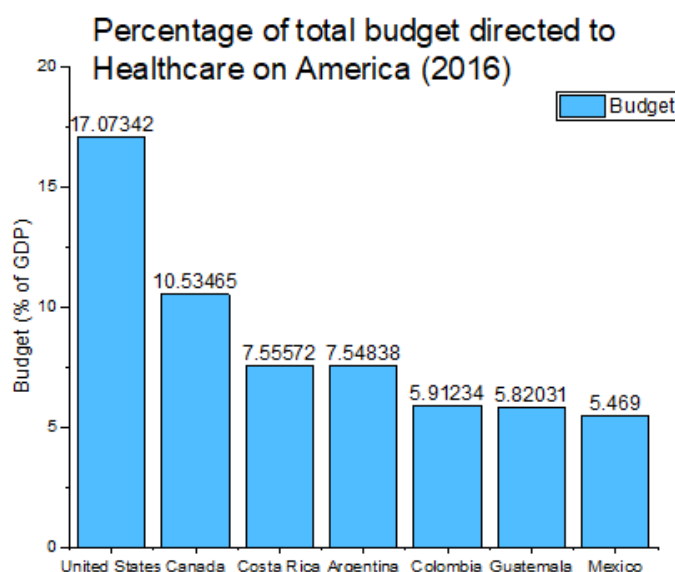


Figure 1.1: *Budget percentage used in health care some American countries in 2016.*

The increasing spread of infectious diseases in developing countries has motivated the development of more affordable devices accessible to a higher number of patients and being able to perform the diagnosis in shorter times; This will allow opportune treatment. The World Health Organization (WHO) has established a set of criteria to guide the development of diagnostic tools for limited resources, introducing the acronym "ASSURED": (1) affordable, (2) sensitive, (3) specific, (4) user friendly, (5) rapid and robust, (6) equipment-free (minimal), and (7) deliverable to end-users [6]. The diagnostic tools that accomplish the previous criteria are considered as Point of Care (POC) devices. POC devices have attracted attention due to the recent advances on fabrication, miniaturization and easy application without requiring the intervention of a laboratory [7, 8] in comparison to conventional detection methods such as cell culture, Polymerase Chain Reaction (PCR) and enzyme-immunoassay [9].

Microfluidic-based devices are prime example of tools which meet the "ASSURED"

criteria, only requiring a small volume of sample and reagents to perform an analysis and diagnosis [9, 10]. The polymer-based fabrication used for microfluidic devices is another advantage for their implementation as disposable diagnostic tool [11]. The centrifugal microfluidic platform or "Lab-on-a-Disc" (LoaD) is one of the most explored devices to be exploited for the mentioned reasons and the reduction of mechanical equipment for its operation.

A Lab-on-a-Disc is a CD-based platform able of moving liquid through microchannels and microchambers by rotating the platform, generating centrifugal pressure on it [12, 13]. The CD platform presented by Kim et al. is an example of LoaD platform destined for electrochemical sensing [14]. The minimal equipment, as well as the easy fabrication, have made this platform to be implemented in POC applications. Gilmore et al. mentioned that an LoaD platform is even suitable for extreme POC applications if the device has robust reagents and reliable storage, inexpensive manufacturing and simple spinning protocols for binary assay results [7].

There are multiple detection schemes that can be employed in microfluidic devices. These detection methods can be classified in optical and electrochemical detection techniques. The centrifugal platform by Kim et al. [14] is an example of device using an electrochemical sensor as detection method. In spite of being versatile in terms of low detection limit and microfabrication, electrochemical techniques still require the implementation and interpretation to the results done by an experienced user. On the other hand, the optical techniques generate binary responses suitable for extreme POC [7, 15]. The use of optical techniques, such as fluorescence, can provide different responses (in form of color) for multiple targets unlike electrochemical techniques which require different set of electrodes for each target.

Immunofluorescence is an optical technique able to detect different antibodies from a sample by using a site-specific ligation while the antibody is labeled with fluorescent compound to detect this interaction. While the detection of antibodies is usually done on ELISA (Enzyme-Linked Immunosorbent Assay)-based arrays, it is time-consuming and requires large quantities of reagents and sample [15, 16]. Peptides microarrays have been developed as an alternative to perform the detection of antibodies, either for epitope mapping or identification of binding interactions between peptides-proteins. The peptides microarrays offer advantages, in comparison to protein arrays [17], such as: easy synthesis and manipulation, highly stable and inexpensive [16, 18].

Peptides-microarray based immunoassay is one of many applications that it is possible to adapt to a LoaD platform. The development and miniaturization of bioanalytical assays on LoaD platform brings multiple features that are required for a POC device: reduction of sample and reagents for immunodetection, detection

of multiple targets on an assay (or multiplexing) and inexpensive fabrication and experimental setup. Automation of the assays reduces human error on the process. The use of active pumps such as electrolysis-induced pneumatic pump can ease the movement of multiple reagents in a test by reducing the implementation of actuators influenced by centrifugal forces and simplifying it. The manipulation of electrolysis pumps via electrical current can enable the programming of movement of each reagent. Up to this date, it has not been reported a LoAD platform designed for automation of a bioanalytical assay using this kind of actuator.

This thesis presents the design and implementation of an electrolysis pump for centrifugal microfluidics and applies the pump for automation of a detection protocol based on a peptide microarray. The work includes the implementation of an immunoassay protocol with reduced footprint adapted for Lab-on-a-Disc platform, the design and implementation of electronic circuit to actuate the pump, the software to wirelessly control the pump, and the implementation of a setup suitable for POC applications.

The chapter 2 of this work shows the state-of-art in the area of electrolysis pumps on microfluidic platforms and automation of immunoassays. The chapter 3 focuses on the background required to understand the developed system. Chapter 4 sets the methodology used for this work and Chapter 5 shows the results, and Chapter 6 presents the main conclusions.

Chapter 2

State of Art

This chapter presents an overview of previous works related to the manipulation of liquids by the use of electrolysis of water as pressure source in microfluidic devices. General designs, materials and measured parameters of platforms that employed an electrolysis pump are covered here. Moreover, this chapter covers previous immunoassays adapted on Load, showing their suitability for POC setting.

2.1 Electrolysis pump on microfluidic Chips

The electrolysis of water, i.e. the production of hydrogen and oxygen by dissociation of water, is a well-known pumping process by its low power consumption, minimum heat dissipation, ease of control and low use of resources to operate [19, 20]. Moreover, since it only requires a pair of electrodes and electrolyte in a reservoir to actuate, it has shown promising potential as pressure source for fluid manipulation within microchannels and chambers networks [21].

Pagonis et al. employed the PCB fabrication technology to create copper electrodes to move a solution with electrolyte through a microchannel by using the same solution for the electrolysis reaction [20]. They reported a linear relationship between electrical current and flow rate in the rate range of $0.34\mu L/s$ to $2.25\mu L/s$. Kim et al. reported a comparison in the pumping and power performance of interdigitated gold electrodes fabricated by microfabrication techniques (lithography and sputtering) and PCB technology. With both fabrications, they got the same flow rate range ($0.167\mu L/s$ to $2\mu L/s$) but the PCB electrodes consumed less power for the system from $2.8mW$ to $32.9mW$ [21]. These works demonstrated that it is possible to reduce fabrication costs by using the typical methods to fabricate metal electrodes for electrolysis. However, the direct contact between the electrolysis solution and the sample in their design, leads to contamination for the biological assays.

Yi et al. presented the use of the electrolysis pump to cyclically deform a PDMS diaphragm to push a drug solution through a cannula. This design has multiple variations where the material of foam in the pump (used to recombine the gases to water in the inactive pumping state) has been changed to platinum-coated nickel and platinum coated carbon fiber mesh [22, 23]. Other version of Yi's pump uses inductive coils to supply power to the electrodes in the pump [24]. Lui et al. [19] presented an electrolysis pump that forces the deflection of a PDMS layer, generating hydraulic pressure in the adjacent chamber filled with liquid. Then, this chamber transfers the pressure to the reagent chamber to push it through a microchannel (**Figure 2.1**). The previous microfluidic devices presented an alternative to avoid contamination for the biological sample and optimize the system for wireless power transfer. However, they are presented as proof-of-concept of a drug delivery system.

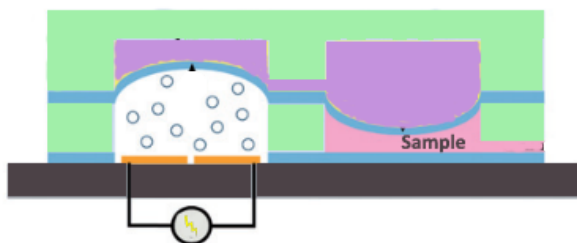


Figure 2.1: *Schematic illustration of mechanism of actuation for mobilization of liquid by deflection of membrane. The electrolysis pump increases the pressure, transferring it through a hydraulic fluid. (Figure by Lui et al. [19] from the Journal Lab on a Chip).*

There are multiple microfluidic devices integrated with electrolysis pumps as pressure source for implantable drug delivery. Li et al.[25] designed a microfluidic device whose electrolysis pump can move 250nL of drug per dose to the eyeball via cannula (**Figure 2.2.A**). Sheybani et al. implanted a microdevice to deliver 19.12 μ L cocaine within 50 minutes by the activation of an electrolysis pump [26]. Gensler et al. presented a microfluidic device implanted in vivo to mice for cancer treatment by actuating an electrolysis pump to mobilize (siRNA)- gold nanorod complexes [27]. A pH sensor with electrolysis pump has also been reported. Sim et al. uses the bubbles generated by the pump to move the sample to the sensing chamber and calculate the pH via electrical resistance depending the amount of bubbles created [28]. Li et al. [29] use multiple electrolysis pumps to move aqueous liquids and oil to create droplets in low-pulsation. Kuo et al. [30] use the electrolysis pump to move a sample with N-Terminal pro-brain-

Type natriuretic peptide (NT-proBNP) to the sensing area where there are electrodes with functionalized antibodies to couple with the target and measure their presence using the capacitance (**Figure 2.2.B**). Most of the electrolysis pumps reported have been used for drug delivery while the ones presented by Sim et al. [28] and Kuo et al. [30] are applied for biological assays. The disadvantage of the use of the electrolysis pump in Lab on a Chip is the presence of bubbles in the surface of the electrodes which acts as a barrier in the medium reducing the gas generation.

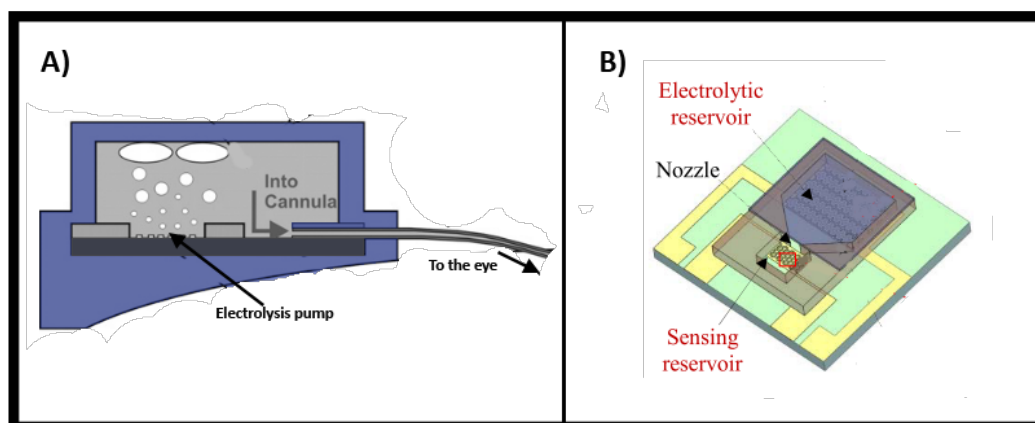


Figure 2.2: *A) Cross-section of ocular drug delivery device using electrolysis gases to pump drug into the eye (Adapted from Li et al. [25] of the journal *Sensors and Actuators, A: Physical*) . B) Schematics of proposed immunosensor which uses electrolysis pump to move sample to be sense by electrodes (Adapted from Kuo et al. [30] of *Proceedings of the IEEE International Conference on Micro Electro Mechanical Systems*) .*

Noroozi et al. [31] demonstrated that the implementation of the electrolysis pump in a Lab on a Disc mobilizes liquid against the centrifugal force in a wide range of rotational speed. The efficiency of electrolysis is not affected in this setting because the bubbles are break down by the centrifugal force. Until now, Noroozi's work has been the only one that has implemented the electrolysis pump and only as a proof-of-concept. **Table 2.** presents a summary about the properties of the works mentioned in this section.

Author	Application	Flow rate range (uL/s)	Electrical current (mA)
Pagonis et al.[20].	Proof-of-concept	0.34-2.25	1.23-12
Kim et al.[21]	Proof-of-concept	0.164-1.255	100-2000
Yi et al.[22]	Proof-of-concept	0.008-0.216	
Yi et al.[24]	Proof-of-concept	0.283-0.616	
Yi et al.[23]	Proof-of-concept	0.003-0.141	
Lui et al.[19]	Proof-of-concept	0.008-0.025	2-18
Li et al.[25]	Ocular drug delivery	7.3(pL/s)-0.116	0.050-1.25
Sheybani et al.[26]	Drug delivery	0.25-2.35	2-13
Gensler et al.[27]	Cancer drug delivery	0.0167-0.1167	0.4-2
Sim et al.[28]	pH sensor		
Li et al.[29]	Droplet formation	0.0167-0.1167	0.1-1
Kuo et al.[30]	Capacitive immunosensor		
Noroozi et al.[32]	Proof-of-concept	0.5-8	5-90

Table 2.1: **Summary of microfluidic devices where the electrolysis pump was implemented.**

2.2 Automation of Immunoassay on Lab on a Disc

The immunoassays on microfluidic devices take great importance by their easy adaptability and optimization of time and costs for POC tests [33]. There have been reported numerous works to demonstrate the feasibility of unit operations (valves and pumps) and CD designs for protocols that don't require the intervention of the user.

Lee et al. reported a LoaD platform that controls the flow of the reagents by ferrowax valves which are melted by a laser diode [34]. The detection of Hepatitis B virus, HBsAg and Anti-HBs was done by using $50\mu L$ of sample and antigen and antibody coated microbeads. Kim et al. used ferrowax valves and electrodes as electrochemical sensor in a LoaD platform for the detection of C-reactive protein (CRP) (required $150\mu L$ of sample), using antibody coated microbeads to couple with the target particle for detection [14]. Park et al. reported the automation of bead-based immunodetection of CRP, cardiac troponin I and NT-proBNP by the use of ferrowax valves [35]; they required $200\mu L$ of sample for the protocol. Even though the use of ferrowax valves guarantee the closed/open behavior to improve the control of the liquid flow, the need of laser complicates the equipment setup for the CD.

Ukita et al. [33] and Ishizawa et al. [36] designed a LoaD platform with three-dimensional microchannel networks and vertical capillaries to control the liquid flow for detection of mouse Immunoglobulin G (IgG); both works used a maximum sample volume of $10\mu L$. Okamoto et al. used a centrifugal microfluidic platform, based on CLOCK-autonomous concept, for the detection of human albumin ($100\mu L$ of sample) in a steady spinning speed [37]. The advantage of CD designs that actuate their valves by centrifugal forces is the simplification of equipment to connect to the platform. However, these valves are susceptible to the rotational speed, having a high probability to leakage.

Thio et al. used a thermo-pneumatic pump, which pushes or pulls the liquid depending of the expansion of air, to automate the sequence of an immunoassay [38]. Wang et al. reported the automation of immunoassay protocol of LoaD platform by the use of flyball governors as valves; they used anti-mouse IgG conjugated with magnetic nanoparticles to concentrate the sample mouse IgG ($40\mu L$) in a specific zone for the capture [39]. Aeinehvand et al. reported the use of aluminium valves (opened by mechanical pressure) and magneto-balloon mixer for sepsis detection by the immunocapture of sTREM-1 ($100\mu L$ of sample) in a LoaD platform [40]. Thiha et al. created a centrifugal setup for optical immunodetection of Dengue in POC setting [41]. These works employed external actuators and sensors to improve the automation of immunodetection of multiple diseases. Aside of Thiha et al., the rest of works require external equipment to operate the detection protocol or require to stop the CD to

actuate the valves. Thiha et al. proposed a useful setup to be used outside of clinical establishments, but it lacks a complete CD design to demonstrate that it can be used for more complex or multiplexed assays.

Noroozi et al. [32] developed a LoaD platform able of running a multiplexed immunoassay by the use of proteins arrays for detection. However, the actuation of siphon channels that they used requires to rotate the CD in very high speed (above of > 3200 RPM). Aeinehvand et al. used elastic tunable valves to control the flux of reagents for a multiplexed detection based on peptides microarray (anti-HA, anti-FLAG, polio, tetanus and *S. aureus*) [42]. This work demonstrated that it is possible to automate an assay protocol that requires multiple reagents in a simple CD design as the case of peptides microarray protocol. The implementation of plastic screws and PDMS cubes benefits the modulation of the valve for the user, determining the burst frequency for each reagent. However, the CD layout requires to consider their implementation, increasing the footprint and layers of thick plastic to conform the tunable valve.

Chapter 3

Background

This chapter presents fundamentals about the operation of Lab-on-a-Disc platform, common fabrication methods and the unit operations (valve and pump) required to implement a peptides microarray-based immunoassay protocol. The chapter covers also background on the "electrified Lab-on-a-Disc" (eLoaD) and the glassy carbon electrodes for electrolysis pumping.

3.1 Lab on a Disc

As one alternative to Lab on a Chip, LoaD platforms exploit the centrifugal forces to manipulate liquids through the CD [43, 44]. These platforms have multiple advantages such as: Minimal amount of instrumentation to manipulate liquids, removal of bubbles and residual liquids, and multiplexing several assays on a single disc. Because of the centrifugal pumping offered by LoaD, it is possible to analyze quite different aqueous solutions independently of their physicochemical properties such as pH, ionic strength and chemical composition [10, 12, 13, 45, 46]. Duffy et al. reported that by varying the channels dimensions in a CD it is possible to achieve a large range of flow rate from 10 nL/s to 100 μ L/s [47].

The LoaD platforms present multiple forces acting on liquids or particles by the presence of centrifugation (denominated as "**intrinsic forces**"). It is important to sub-classify the intrinsic forces into two: Pseudo-forces (Forces available only on rotating systems) and non-pseudo forces (Forces that appear on rotating and non-rotating systems) [13, 45]. The pseudo-forces comprise the centrifugal force (F_ω), Coriolis force (F_c) and Euler force (F_e) [43, 44, 48]. The centrifugal force, which acts radially outward of the CD, is the main force that provides the movement of the liquid and is represented as:

$$F_\omega = \rho r \omega^2 \quad (3.1)$$

where ρ is the mass density of the fluid, r is the actual position in the CD respect with the center, ω is the angular rotational frequency. **Eq. 3.1** can be converted to its scalar pressure equivalent by integrating between the points r_1 and r_2 :

$$P_\omega = \int_{r_1}^{r_2} \rho r \omega^2 dr = \frac{1}{2} \rho \omega^2 (r_2^2 - r_1^2) = \frac{1}{2} \rho \omega^2 \Delta r \bar{r} \quad (3.2)$$

where r_1 is the distance from the center to the upper meniscus of the liquid and r_2 from the center to the bottom meniscus of the liquid, Δr is the difference between r_1 and r_2 and \bar{r} is the average distance of the points r_1 and r_2 .

The Euler force is generated perpendicularly to the centrifugal force when the acceleration is different to zero, obtaining its direction equal to the CD rotation. This force is given by:

$$F_e = -m \frac{d\omega}{dt} \times r \quad (3.3)$$

where $\frac{d\omega}{dt}$ is the change of angular velocity per unit time and m is the mass of liquid.

The Coriolis force is dependent to the velocity of the liquid and its direction is against to the CD rotation. The equation is represented by:

$$F_c = -2m\omega \times v \quad (3.4)$$

where v is the velocity of the liquid moving in the disc. The three pseudo forces are represented visually in **Figure 2.1** [13, 44].

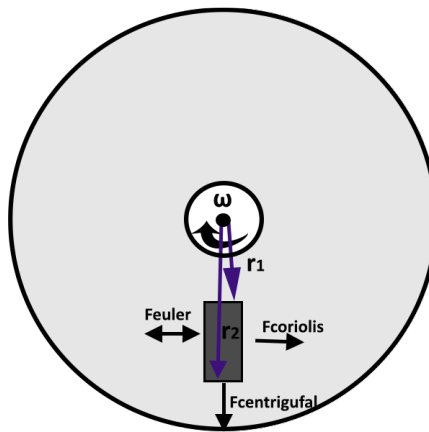


Figure 3.1: *Pseudo-forces in Load platforms.*

The non-pseudo forces appear in either the presence or absence of centrifugation. The viscous pressure (P_v) and capillary pressure (P_{cap}) are some pressures derived of non-pseudo forces that play a major role in CD platforms [45, 49]:

$$P_v = -R_{hyd}q \quad (3.5)$$

$$P_{cap} = \frac{4\cos\theta_c\gamma_{la}}{D_h} \quad (3.6)$$

where R_{hyd} is the hydraulic resistance (proportional to the dynamic viscosity μ), q is the volumetric flow rate, θ_c is the liquid contact angle, γ_{la} is the liquid-air surface energy and D_h is the channel hydraulic diameter.

Finally, it is indispensable to consider the velocity of liquid v seen in **Eq 3.4** and volumetric flow rate q in **Eq 3.5**. These variables are calculated by [13]:

$$v = \frac{D_h^2\rho\omega^2\bar{r}\Delta r}{32\mu L} \quad (3.7)$$

$$q = vA \quad (3.8)$$

where L is the length of liquid column in the microchannel and A is the cross-sectional area of the microchannel.

3.2 Unit operation: Active valves and RTPV valve

As one of the most critical unit operation on Load, valving controls the flow of the liquid through the microfluidic network. The valves are components that enable parallel control of multiple liquids on spinning discs to perform multi-step processes [48, 49]. The burst frequency is one the most important properties to consider during the design of a CD valve because that value is determinant for the spinning speed protocol for the assays in the platform [12, 45].

A valve can be classified either as active or passive depending of the nature of the actuation source. While the passive valves are controlled using centrifugal forces, the active valves require external means for their actuation such as electrical current, heat, pneumatic force, etc. [45]. Even if the use of active valves need external mechanism for the CD, they are independent to the spinning protocol (reduce the possibility of leaking).

Choi et al. reported a valve made of polyethylene substrate which is opened by the heat up of an external laser [50]. Amasia et al. used ice valves actuated by thermoelectric modules for the adaptation of PCR test [51]. Aeinehvand et al. reported a method to

integrate mechanical valves during the fabrication of plastic CDs which can be actuated by break them directly [52]. Multiple works presented by Cai et al. have presented the use of a flyball governor to maintain the PDMS valve closed by mechanical pressure [53, 54]. All these valves present disadvantages for POC settings such as the use of bulky equipment [50, 51, 53, 54].

The reversible thermo-pneumatic valve (RTPV) [55] is a valve integrated by an enclosed air chamber in contact with an elastic membrane. When the valve receives external heat, the enclosed air will expand inside of the chamber. The expansion of air will deflect the membrane, blocking a microchannel and therefore the liquid flow. The **Figure 3.2** shows a schematic of the composition of the valve, as well as the behavior of the liquid flow during the actuation. **Figure 3.2.b** displays the predominance of pressure generation by the expansion of heating air over the centrifugal pressure in the liquid, blocking the flow. However, either the valve is cooled down, the centrifugal pressure can overcome the pressure given by the valve and the liquid flow continues (**Figure 3.2.c**).

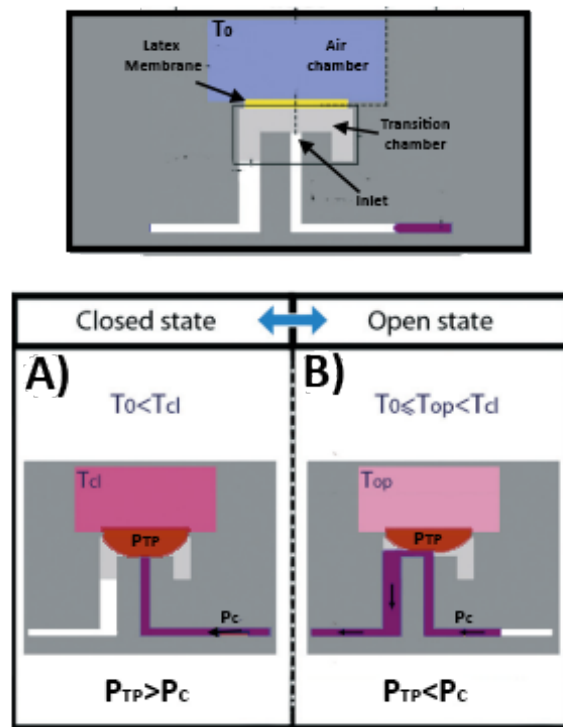


Figure 3.2: *Schematic illustration of mechanism of the Reversible Thermo-pneumatic Valve. a) Parts of the valve. b) Closed state when it is receiving heat. c) Open state when it is in room temperature (Figure by Aeinehvand et al. [55] from the journal Lab on a Chip).*

The differential pressure generated in the RTPV is composed of two variables: the pressure induced by the expansion of air (ΔP_{TP}) and the pressure required to deflect the membrane (P_m). The difference of pressure is given by:

$$\Delta P_{RMV} = \Delta P_{TP} - P_m \quad (3.9)$$

The pressure P_{TP} is modeled by the ideal gas law:

$$\Delta P_{TP} = \frac{nRT}{V_{TP}} - \frac{nRT_0}{V_0} \quad (3.10)$$

where n is the number of moles, R is the ideal gas constant, T_0 and T are the room temperature and actual temperature, respectively, and V_0 and V_{TP} are the volume of air in the closed chamber at room temperature and actual temperature, respectively. The change of volume by the heating in the chamber (V_{TP}) is given by:

$$V_{TP} = V_0 + V_{mb} = V_0 + \frac{2}{3}\pi r_m^2 z \quad (3.11)$$

where r_m is the radius of the membrane in the chamber, V_{mb} is the expanded air volume and z is the distance between the membrane and the inlet of the microchannel. Assuming that $V_0 \geq V_{mb}$, the expression in **Eq. 3.10** can be reduced to one element:

$$\Delta P_{TP} = \frac{nRT}{V_{TP}} \quad (3.12)$$

The pressure required to deflect the membrane P_m is defined by the membrane bulge equation:

$$P_m = C_a \frac{Ejz^3}{r_m^4(1-\nu)} - C_b \frac{\sigma_0 jz}{r_m^2} \quad (3.13)$$

where E is the membrane's Young's modulus of elasticity, ν is the Poisson's ratio, j is the thickness of the membrane, σ_0 is the initial stress and C_a and C_b are constants related to the geometry of the membrane.

The expressions **Eq. 3.12** and **Eq. 3.13** are substituted into **Eq. 3.9** to obtain the pressure of the valve:

$$\Delta P_{RMV} = \frac{nRT}{V_{TP}} - \left(C_a \frac{Ejz^3}{r_m^4(1-\nu)} - C_b \frac{\sigma_0 jz}{r_m^2} \right) \quad (3.14)$$

When a higher temperature T is provided to the valve, it can increase the pneumatic pressure. On the other hand, increasing the angular rotation in the platform (see in **Eq. 3.2**) can aid the centrifugal pressure to overcome ΔP_{RMV} . In other words, the

OPENED/CLOSED state in the valve will depend on the predominant pressure.

3.3 Electrolysis of water: Theory

The water electrolysis initiated when a water molecule passes through a electrical current to be separated in hydrogen and oxygen components [56]. These components are obtained in their gaseous phases. A water electrolysis unit consists of two electrodes (anode and cathode), power supply and an electrolyte [57]. The electrodes are named depending on which output of the direct current (DC) supply are connected to them: the electrode connected to positive is the anode and the one connected to negative is the cathode. **Figure 3.3** shows an example of the elements used during the water electrolysis.

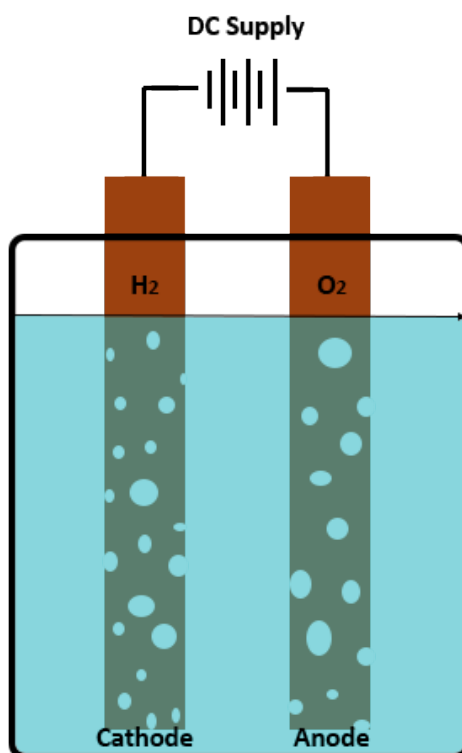
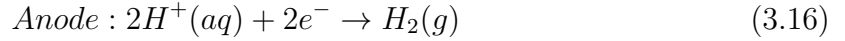
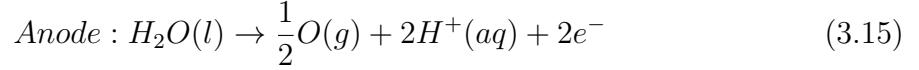


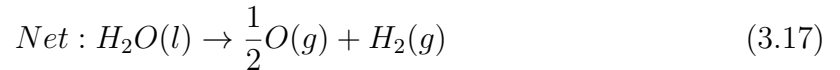
Figure 3.3: *Schematic illustration of the basic components that are involved during a water electrolysis process.*

To initiate the electrolysis process, the DC current is applied to the electrodes. The current passes through to break the water molecules to form hydrogen and hydroxide ions, continuing with the oxidation-reduction reactions. During the reduction reaction, electrons flow from the negative terminal of the power supply to the cathode where

they are combined with hydrogen ions to form hydrogen atoms. On the other hand, hydroxide ions move toward the anode where they drop electrons forming half of oxygen atom (oxidation reaction) [21, 57, 58]. The reactions in the anode and cathode can be expressed as:



The sum of **Eq. 3.15** and **Eq. 3.16** leads to an overall equation for the water electrolysis:



where the overall voltage to decompose the water is 1.23 V [56, 57, 59]. Because of the high resistive nature of the water, it is added an electrolyte to increase the conductivity in the solution. The conductivity in the electrolysis is a key parameter to get a high efficiency in the gas generation. To achieve this, the system has to overcome resistive barriers to reduce the waste of power. **Figure 3.4** shows the typical resistances that interact in the electrolysis reaction: where R_l and R_i are the resistances generated by

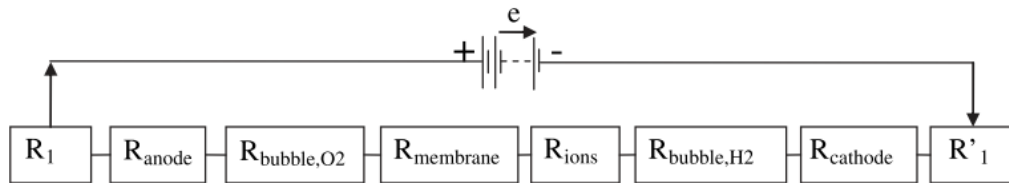


Figure 3.4: *Electrical circuit analogy for resistances presented in water electrolysis (Figure from Zeng et al. [57] from the journal Progress in Energy and Combustion Science).*

wiring and connections with electrodes, R_{anode} and $R_{cathode}$ are resistances due to the overpotential of the oxygen and hydrogen evolution reaction respectively, $R_{bubble,O2}$ and $R_{bubble,H2}$ are originated by the bubbles in the surface of each electrode and R_{ions} is the resistance provided by the electrolyte.

3.4 Unit operation: Electrolysis pump

Noroozi et al. reported the implementation of water electrolysis as a pump to mobilize liquid against the centrifugal force [31]. The accumulation of gas in an enclosed embedded network of chambers in the CD generates an increasing pneumatic pressure

enough to push liquid to the next chamber. The microfluidic network designed for the electrolysis pump is composed of: electrolysis chamber, loading chamber, destination chamber and microchannels that connect them to each other. **Figure 3.5** displays the essential parts of the electrolysis pump. The microchannel that connects the loading chamber with the destination chamber is designed as a siphon channel to maintain the liquid in its chamber by influence of the centrifugal force.

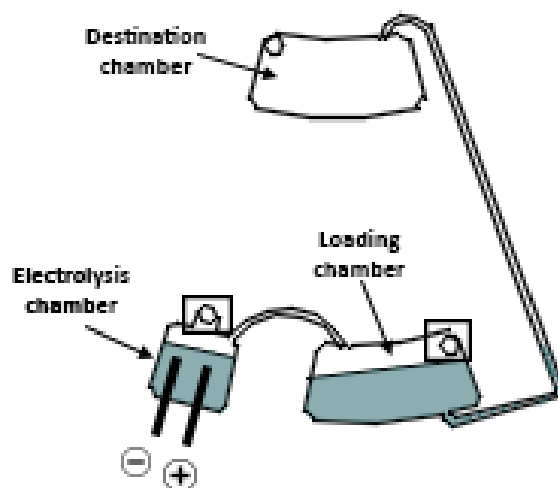


Figure 3.5: *Schematic illustration of the microfluidic network that integrates the electrolysis pump.*

The operation of the pump, after filling the electrolysis chamber (solution with electrolyte) and loading chamber (sample) and sealing the inlets and edges of the electrodes, can be described by the following steps:

1. The CD is rotated, localizing the electrolysis solution and sample in the bottom of their corresponding chambers. As it has been explained, the sample is not able of moving through the siphon channel because of the centrifugal force (**Figure 3.6.a**).
2. The electrical current passes through the electrodes that are in contact with the electrolysis solution, generating the gases. The gases flow through the microchannel into the loading chamber and the accumulation increases the pressure applied to the sample. When the pneumatic pressure by the gases overcomes the centrifugal pressure, the sample travels through the siphon channel (**Figure 3.6.b**).
3. The sample arrives to the destination chamber, filling it continuously (**Figure 3.6.c**).

4. All the sample volume arrives to the chamber and the deactivation of the pump can be done (**Figure 3.6.d**).

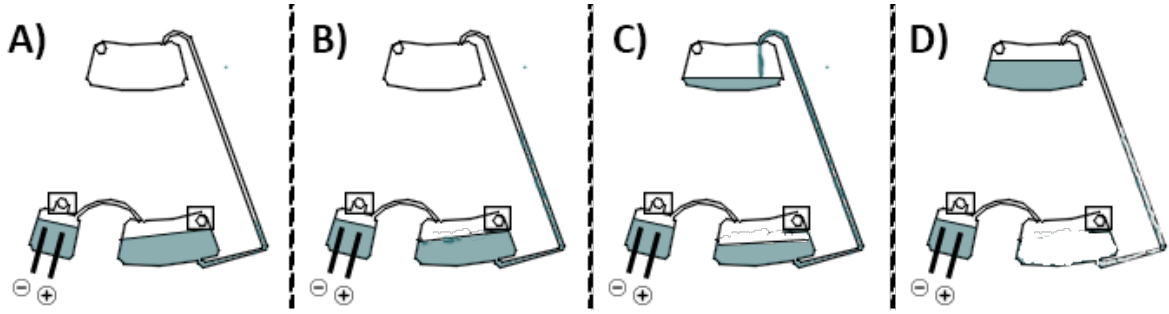


Figure 3.6: *Schematic illustration of the electrolysis pumping process.*

To model the pneumatic pressure and flow rate that the electrolysis pump can create, it is used the Faraday's law for electrolysis by applying a constant current:

$$n_{gas} = \frac{3}{4F} \int_0^t I d\tau = \frac{3}{4F} It \quad (3.18)$$

where m_{gas} is the molar value of generated gas, F is the Faraday constant, I the applied electrical current and t the duration of electrolysis. It is possible to substitute the ideal gas law (**Eq. 3.10**) into **Eq. 3.18** to estimate the gas expansion and pressure:

$$\frac{V}{t} = \frac{3RT}{4FP} I \quad (3.19)$$

where P is the gas pressure, V is the gas volume, R is the universal gas constant and T is the absolute temperature in the gas. It is expected that the gas volume increases while it is not obstructed. When the gas is confined in the chambers, the pressure starts to increase and initiates the mobilization of the sample.

Following the design seen in **Figure 3.5**, the mathematical model can still be developed considering that the gas pressure has to overcome the centrifugal pressure which the sample is subject to. Using the previous statement, it is possible to determine parameters required to analyze the behavior of the sample in this situation. **Figure 3.7** displays a schematic illustration of the microfluidic network and the parameters related to distances between the center of the CD and the meniscus of the sample volume.

Following **Figure 3.7**, the variable z is used to denote the actual distance between the center of the CD and the upper meniscus in the loading chamber. z can be represented as $R_1 + \Delta z$ and using **Eq. 3.2**:

$$P(z) = P_{atm} + \int_{R_1 - \Delta x}^z \rho r \omega^2 dr = P_{atm} + \frac{1}{2} \rho \omega^2 [z^2 - (R_1 - \Delta x)^2] \quad (3.20)$$

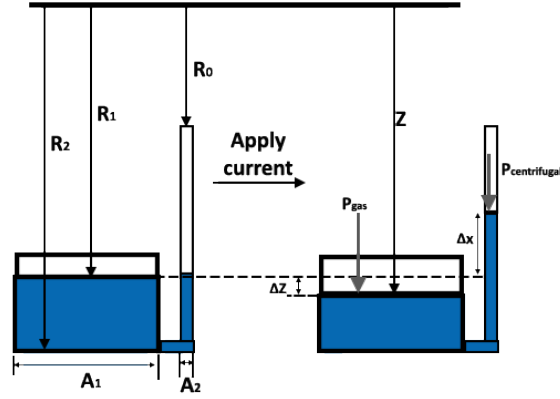


Figure 3.7: *Illustration to highlight the parameters required to analyze the actuation of the electrolysis pump.*

where P_{atm} is the atmospheric pressure, R_1 is the initial distance from the center to the upper meniscus in the chamber, Δx is the change of distance of the upper meniscus of the liquid column respect with the initial position, ρ is the mass density of the liquid and ω is the angular rotational frequency. **Eq. 3.20** is valid when the liquid column has not reached the highest point in the siphon channel (R_0). The period between the beginning of the pumping actuation to the moment when fluid reaches R_0 is known as **”transient” pump regime**. As the liquid reaches the highest point in the channel, Δx becomes constant to $R_1 - R_0$. The new regime, called **Steady-state pumping regime**, is represented as:

$$P(z) = P_{atm} + \frac{1}{2}\rho\omega^2[z^2 - R_0^2] \quad (3.21)$$

To estimate the sample flow rate, it is important to consider two facts: the actuation complies the continuity equation $A_1\Delta z = A_2\Delta x$ (A_1 is the cross sectional area of loading chamber, A_2 is the cross sectional area of siphon channel) and there is an initial air volume in the chambers before the pumping (V_0). By coupling the **Eq.3.18** and **Eq.3.19** and considering **Eq.3.20**, the sample flow rate can be estimated by:

$$Q_z = \frac{3RT_{EP}I}{4F} \frac{\Delta V}{P(z)V - P_{atm}V_0} \quad (3.22)$$

where T_{EP} is the temperature in the electrochemical cell, ΔV is the volume displaced sample (being $\frac{(R_1 - \Delta x)}{A_2}$ and $\frac{(z - R_1)}{A_1}$ if the pumping is in transient and steady-state regime respectively) and V is the volume of air and electrolysis gases occupied in the chambers ($V_0 + \Delta V$).

3.5 Glassy carbon electrodes

Glass-like carbon, or glassy carbon, is known to be an excellent electrode material given its electrical and electrochemical properties, stability, low cost and biocompatibility [60, 61]. There are multiple methods on Carbon MEMS (C-MEMS) to fabricate glass-like carbon from polymer derived carbons. Glass-like carbon microstructure contains graphitic and amorphous zones, being equal to glassy carbon [60, 61, 62]. SU-8 is the material of choice, in comparison with AZ and Shipley products, when it is required to pattern structures with height above of $10\mu m$ [63].

Glassy carbon electrodes are made using two processes: Photolithography and pyrolysis [64]. Photolithography consists of patterning with UV light to change the chemical composition in the exposed zone. First, the photoresist (SU-8) is deposited on a substrate. Then, heat is applied to the precursor in a step called soft bake to evaporate the solvent. The material is exposed to light to start a cross-linking reaction, making less soluble to the developer. A second step of heat called post-exposure bake is applied to finish the cross-linking reaction and finally, the material is submerged to developer to obtain the desirable patterning [61, 63]. Pyrolysis, or thermochemical decomposition, is a process where an organic material is heated to high temperature in an inert atmosphere to obtain solid residues with high content of carbon. This process is the determinant for the majority of properties in the glassy carbon [62, 64, 65]. To create the inert atmosphere, flow of nitrogen (N_2), argon (Ar) and forming gas (95% N_2 and 5% H_2) are commonly used to avoid the loss of the structure by the oxygen. The pyrolysis can be divided in three steps [63]:

1. **Pre-carbonization.** Below of $300^\circ C$, the molecules of solvent and unreacted monomers are eliminated from the material.
2. **Carbonization:** From 300 to $500^\circ C$, oxygen and hydrogen are eliminated from the precursor causing a loss of mass. From 500 to $1200^\circ C$, hydrogen and oxygen are completely eliminated and aromatic network is forced to be interconnected.
3. **Annealing:** Above of $1200^\circ C$, there is a gradual elimination of structural defects and impurities.

It is known that the final temperature used during the pyrolysis determines the degree of carbonization, changing the electrical and mechanical properties [60, 61, 63]. **Figure 3.8** shows examples of glassy carbon structures fabricated by the processes mentioned previously. **Table 3.1** enlists some properties of commercial glassy carbon electrodes, by Sharma et al. [66].

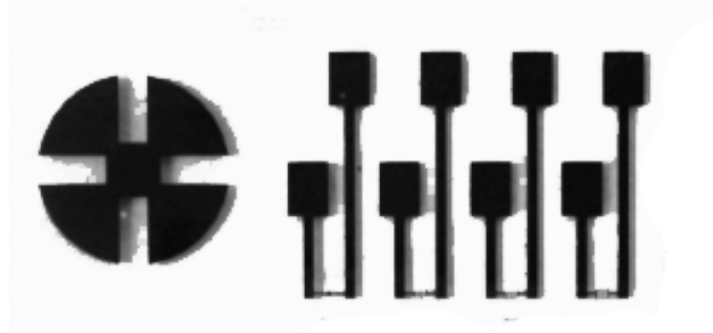


Figure 3.8: *Glassy carbon structures obtained by pyrolysis. Fused silica was employed as substrate to maintain transparency, required for microfluidic platforms (Photo by Pilloni et al. [65] from Journal of Micromechanics and Microengineering).*

Property	Value
Young's Modulus	20-40 GPa
Poisson's ratio	0.15-0.17
Density	1.3-1.55 g/cm^3
Electrical resistivity	10-50 $\mu\omega m$
Thermal expansion coefficient	$(2 - 3.4) \times 10^{-6} K^{-1}$

Table 3.1: Properties of commercial glassy carbon electrodes.

3.6 electrified Lab on a Disc (eLoaD)

Lab on a Disc platforms have been extensively researched as bioanalytical devices using only rotational forces to implement complex protocols. However, some bioanalytical assays demand the implementation of electrical actuators and sensors on the CD. Slip rings have been employed to supply electrically the platform during the spinning, but this equipment has disadvantages for its use in POC setting: Addition of friction for the motor, complicated motor setup for the user, limited number of electrical connections and short lifespan [67].

It has been presented some alternatives to supply a platform in accessible ways. Joseph et al. developed a micro-power generator for centrifugal platforms using magnet sets and coils to supply power to a heating system [68]. Zhu et al. reported the use of a microcontroller supplied by inductive coupled coils to control micro servomotors to change the secondary direction of rotation of lab on a chips [69]. Hofflin et al. reported a wireless power transfer system able to supply 2.4W to a microcontroller in a CD

platform. This system gives versatility to add multiple printed circuit boards (PCB) with different actuators and sensors depending of the application [67].

Torres Delgado et al. redesigned the power regulator (DC-DC converter and power measurement) and microcontroller and its modules to increase the power supply and to adapt the microcontroller to simplify the addition of electrical components [70]. This electrical platform is known as ”**electrified Lab on a Disc**” (eLoaD).

The eLoaD platform is divided into four main modules available for all the LoaD protocols[71]:

1. **Wireless power receiver:** Using a static inductive coil as transmitter and a rotating coil in the eLoaD as receiver, it is possible to supply the entire system constantly while the distance between them is less than $15mm$. The Qi power receiver module is able of obtaining an output of $5V$ and a maximum power of $5W$.
2. **Microcontroller:** Based on the Arduino micro board, the module facilitates the control of LoaD experiments by pre-programmed protocol. The module provides multiple outputs to activate actuators, as well as inputs to recollect data from the sensors. Each port can provide $5V$ with a maximum current of $20mA$.
3. **SD-card:** Module used to record data from the microcontroller for further analysis.
4. **Low energy Bluetooth:**The eLoaD platform can provide continuous feedback by the transmission of data via Bluetooth, either to a computer or a smartphone.

Table 3.2 displays the amount of power used for each module, allowing the use of $3.6W$ for the desirable actuators and sensors for the assays [48].

Module	Power (mW)
Qi transmitter: Transmitted power	5000
On-disc power: Received power (80%)	4000
Arduino microcontroller consumption	190
Bluetooth and SD card consumption	200
Energy available for application	3610

Table 3.2: Power management of the eLoaD disc for centrifugal microfluidic applications.

The implementation of the eLoaD platform in CD application has been reported. Delgado et al. employed a photomultiplier to measure the change of color by tagged chemiluminescent antibodies during ELISA assays [72]. Also, Torres Delgado et al.

reported the capability of control 128 heaters embedded in a PCB connected to the eLoaD for the actuation of centrifugo-pneumatic valves [73]. The activation of the heaters was possible by sending the commands from a tablet via Bluetooth.

3.7 Peptides Microarrays

Microarrays consist of immobilized biomolecules spatially addressed on solid substrates, microwells or arrays of beads. This kind of arrays typically comprise hundreds to thousands of distinct peptide sequences, being useful for parallel or multiplexed diagnosis. [17, 74]. Aside of the stability, easy synthesis and inexpensive fabrication offered by the peptides microarrays [18], they allow multiple analysis techniques such as fluorescence, resonance spectroscopy and mass spectroscopy [17]. **Figure 3.9** shows an example of fluorescence images of some peptides microarrays with labelled target attached, denoting the change of density of peptides.

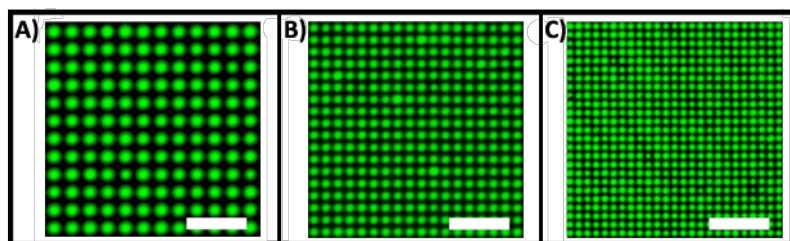


Figure 3.9: Fluorescence images of biotin patterns stained with labelled streptavidin: d) 150 mm (4,444 spots per cm^2), e) 100mm (10,000 spots per cm^2), f) 75mm (17,777 spots per cm^2) (Figure from Loeffler et al. [75] from the journal Nature Communications).

The general scheme of a common protein/peptide array experiment is provided by the **Figure 3.10**: A set of ligands (antigen or antibody) arrayed in a substrate are washed and blocking to avoid reaction on undesirable sites. Then, the sample containing multiple targets (and unrelated molecules) is probed. If an interaction between ligand-target molecule occurs, a signal will be revealed in the analysis methods previously mentioned. This kind of experiment follows the same procedure as the "Enzyme-linked immunosorbent assay" (ELISA) [18, 76]. Depending of which molecule is the ligand and the intervention of secondary targets, the ELISA or immunoassay test can be categorized into 4 types:

1. **Direct ELISA**. Using an antigen as ligand on the substrate, the signal is generated when the corresponding antibody (labelled by an enzyme to visualize) is coupled to it.

2. **Indirect ELISA.** Using an antigen as ligand, the primary antibody (target) attached first. Then, a secondary antibody (labelled to generate signal) attached to the primary one.
3. **Sandwich ELISA.** Using a capture antibody as ligand on the substrate, the coupling is done when the antigen attached to it. Then, a primary antibody attached to the antigen and finally, a second antibody (labelled with an enzyme) unites to the chain.
4. **Competitive ELISA.** This test uses an inhibitor antigen which will compete with the target antigen to couple to the primary antibody. The intensity of the signal is inversely proportional to the amount of antigen of interest.

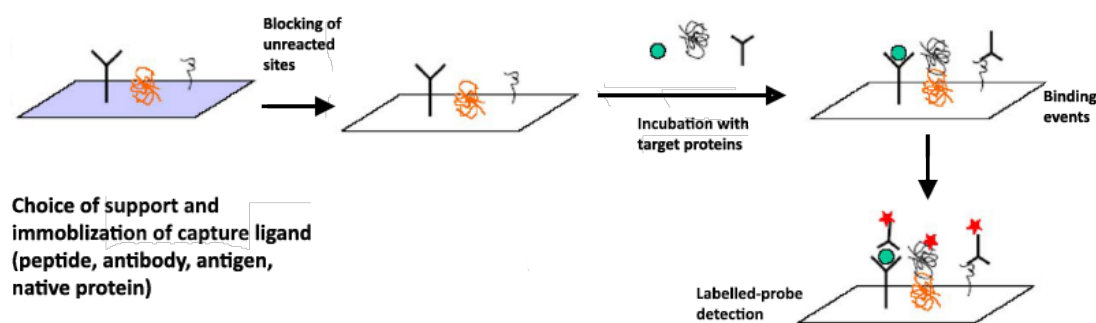


Figure 3.10: *Schematic illustration showing the typical steps in a peptides microarray experiment. After blocking and washing the surface of the substrate, the sample is probed for the incubation step. If a coupling ligand-target occurs, a signal is generated (Figure by Cretich et al. [18] from the journal *Biomolecular Engineering*).*

There are two methods to synthesize peptides in an array format: Merrifield solid-phase and *in situ* synthesis. For purposes of the work, it is only explained the *in situ* techniques. The *in situ* synthesis consists of growing peptides sequences on the substrate layer by layer until the desired length is achieved. It is employed amino acids which are coupled to pre-programmed sites across to the surface [17, 74]. This method has three approaches to create the arrays successfully: SPOT, photolithography and particle-based synthesis.

The SPOT method utilizes Fmoc-protected amino acids to synthesize peptides in directly on a membrane support. After using solutions containing amino acids and reagents on specific locations, the membrane is washed off generating multiple iterative

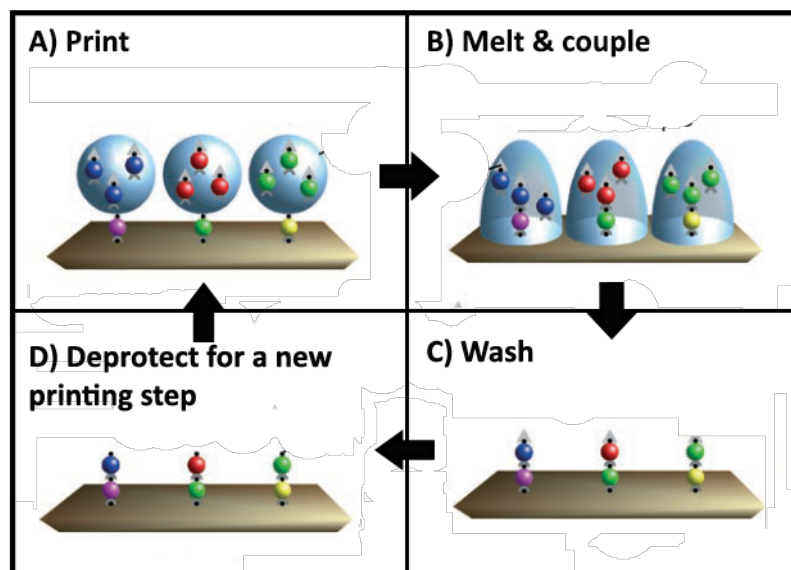


Figure 3.11: *Particle-based synthesis.* a) Laser printer transfers Fmoc amino-acids to solid support. b) Particles are melted, enabling coupling reaction. c) The surface is washed to d) repeat the process until generate the required peptide sequence (Figure by Stadler et al. [77] from the journal *Angewandte Chemie - International Edition*).

cycles. The photolithographic method uses light to direct peptide synthesis on a solid support, employing masks to select the zones destined for specific growing peptide [17].

The particle-based synthesis is a technique derived of the SPOT method but instead of depositing the solutions with liquid handler, 24-ink laser printer transfers toner particles (containing Fmoc protected amino acids) in a solid form. Then, the particles are melted in the surface, allowing the coupling reactions to occur. Finally, the surface is washed off to start the next round of depositions of particles to create the peptide sequence [17]. The **Figure 3.11** displays visually the peptide synthesis sequence by using the particle-based synthesis. Stadler et al., and further the company PepperPrint, employs this method to create arrays with high density [77].

Chapter 4

Materials and methods

The project was composed of two phases that are listed below and demonstrated by details in the flowchart in **Figure 4.1**. Each phase consisted of the design and fabrication of CD platforms with an electronic system developed to investigate and characterize the performance of the electrolysis pump for bioassay automation:

1. **Phase 1: Characterization of electrolysis pump's flow behavior.** In this phase the centrifugal-based electrolysis pump was optimized to provide predictable or controlled flow rates at different CD spin speeds using glassy carbon electrodes. Moreover, the modulation of electrical current has been tested during the flow rate characterization to check the electrical limitations on the system.
2. **Phase 2: Automation of peptides microarray assay.** In the second phase, CD platforms, an electrical circuit and an android application were developed and optimized to automate a peptide-microarray based immunoassay for HA detection.

In this chapter, the integration of the electrolysis pump and RTPV valve implemented on centrifugal microfluidic devices, general CDs' layout, and the development of mobile application, electrical circuit and GC electrodes are detailed and demonstrated. Afterwards, the experiments performed to characterize the pump behavior (phase 1) and to automate the immunoassay (phase 2) are detailed.

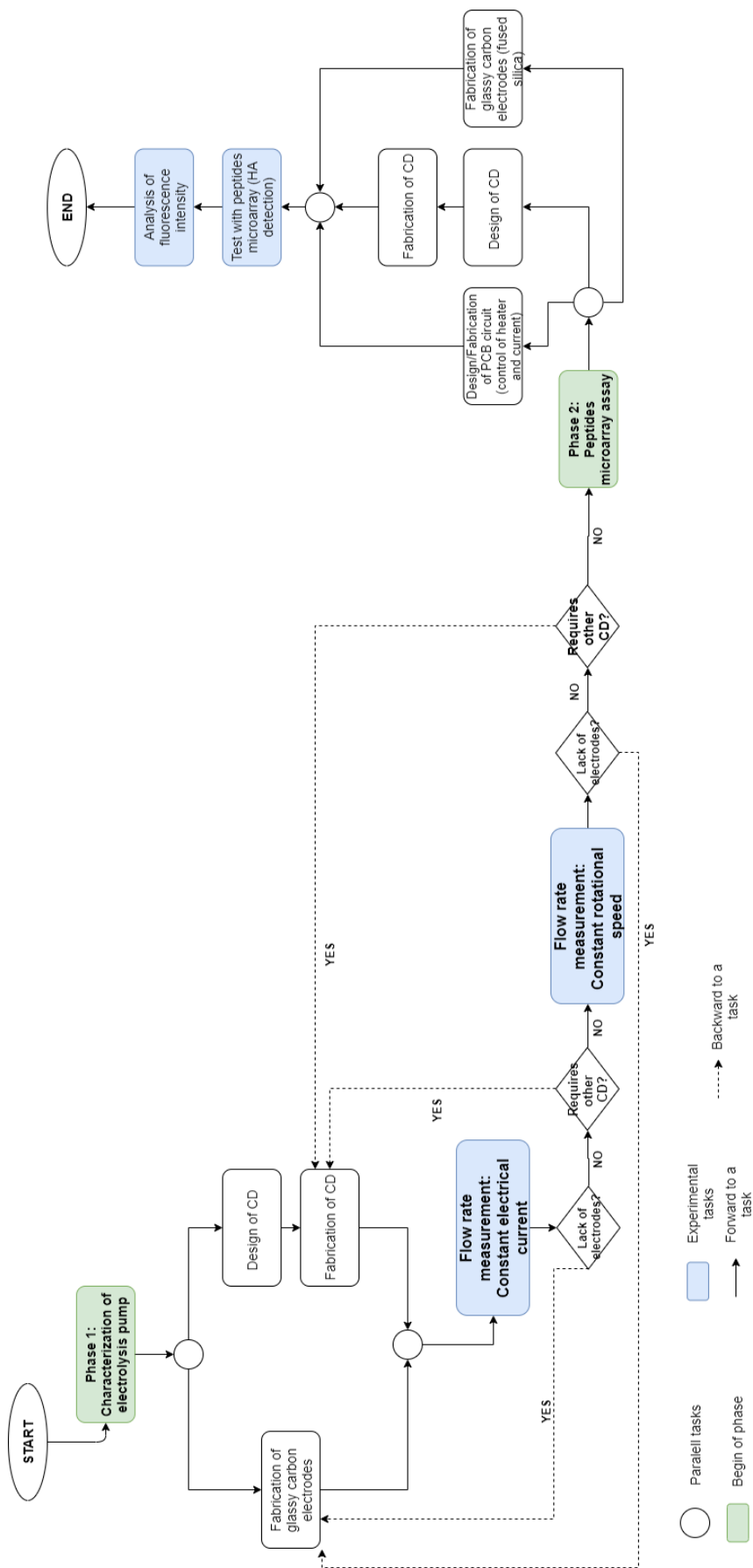


Figure 4.1: Block diagram displaying the flowchart structured for the project in multiple phases.

4.1 Unit operations design: Electrolysis pump and RTPV

Electrolysis pump design

The microfluidic network (arrangement of chambers and channels) introduced by Noroozi et al. [31] (**Figure 3.5**) was adapted for this work. To make the best use of the limited disc space, the position of the siphon channel was modified to reduce footprint in the device. Inspired by Thio et al. [78] and Ishizawa et al. [36], the siphon channel was formed by stacking acetate and pressure sensitive adhesive (PSA) above of the sample chamber, acquiring a 3D orientation in a lateral view. The **Figure 4.2.A** shows the top and side view of an electrolysis pump highlighting the layers required to form the 3D siphon channel. The **Figure 4.2.B-D** displays the movement of the sample after the activation of the electrolysis pump, repeating the transient and steady-state pumping regime seen in the **Figure 3.6**.

There were two parameters to consider during the pump design to avoid undesirable actuations by changes of centrifugal speed: the width of the siphon channel has to be very small (considering the **Eq.3.6**) and the length of the siphon channel has to be large to make sure that the meniscus of the liquid column does not overcome the highest point in the siphon. The smallest channel width that the employed fabrication equipment can achieve is $0.7mm$.

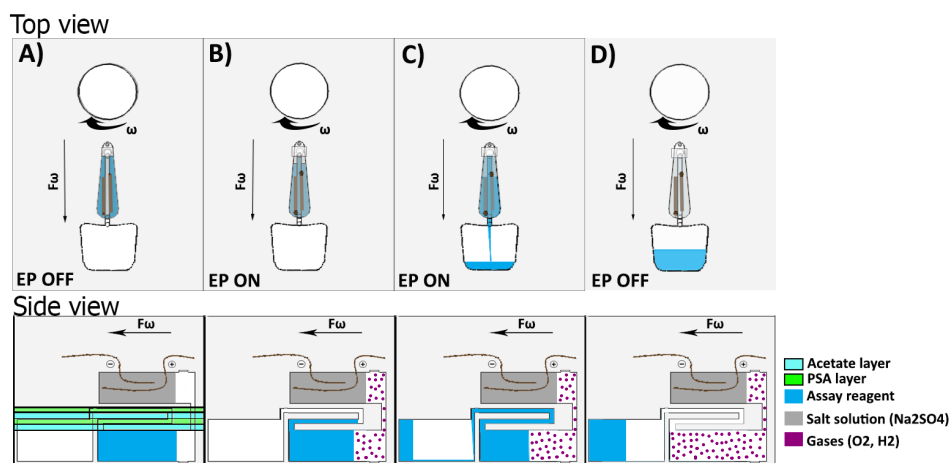


Figure 4.2: *The actuation of the remodeled miniaturized electrolysis.*

Reversible Thermo-pneumatic valve design

The RTPV valve was added to the CD platforms for multiple time opening and closing of an intake between a detection and waste chamber. The radius (r_m) used for the enclosed air chamber in the valve is 5mm , the separation between inlet and the membrane is $50\mu\text{m}$ and the membrane material used is Polyvinyl chloride (PVC) film. The burst frequency required to open the valve with these features is **25 Hz** after activating the heater, data obtained by testing the valve integrated on the CD platform shown in **Appendix A**. The **Figure 4.3** shows a schematic in top view of the RTP Valve. The **Table 4.1** enlists the parameters considered during the electrolysis pump and RTPV design as well as theoretical modeling. The parameters are used to evaluate the performance of the valve using **Eq.3.14** and **Eq.3.22**.

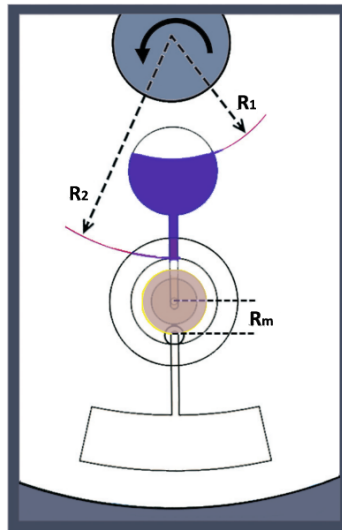


Figure 4.3: *Schematic of the Reversible Thermo-Pneumatic Valve, highlighting the size used for the enclosed air chamber r_m (Figure by Aeinehvand et al. [55] from the journal Lab on a Chip).*

4.2 CD designs and fabrication

Two microfluidic platforms were created for conducting experiment in the first phases of this project. The phase 1 CD was designed for characterization of the flow rate of the electrolysis pump. The phase 2 CD was developed for automation of an immunoassay based on peptides microarray. The microfluidic discs were assembled through layer-by-layer (following the method proposed by Aeinehvand et al. [52]) using the next polymers:

2mm transparent polymethyl methacrylate (PMMA), 1mm transparent polycarbonate (PC), 50 μ m pressure sensitive adhesive (PSA), 70 μ m acetate and 200 μ m polyvinyl chloride (PVC) film. The CD layouts were designed using AutoCAD software (AutoDesk Inc., CA, USA). The micro-features formed in the PMMA and PC layers were cut using the CNC laser model STM-L1390B (STM Robotics, Mexico) and the channels/intakes were cut in the Acetate and PSA layers using the cutter plotter GRAPHTEC CE6000 (GRAPHTEC America Inc.,CA,USA).

Phase 1 CD design

The breakdown of the microfluidic disc "Phase 1 CD" containing two Acetate layers, two PSA layers and one PMMA layer is shown in **Figure 4.4.A**. From the bottom to the top, the first layer (Acetate) contains the holes required to connect the glassy carbon electrodes to the electrolysis chamber. The second layer (PSA) contains the channel that connect the electrolysis chamber with the sample chamber. The third layer (PMMA) contains the sample, electrolysis and destination chambers and measurement lines next to the siphon channel. The fourth layer (PSA) has the siphon channel that connect the sample and destination chambers. The last layer (Acetate) encloses the electrolysis chamber and contains the inlets to all the chambers in the platform.

Phase 2 CD design

The breakdown of the microfluidic disc "Phase 2 CD" containing four Acetate layers, four PSA layers and one PC layer is shown in **Figure 4.4.B**. The CD was designed to adapt the immunoassay using peptides microarray while optimizing the number of layers required for the fabrication. Also, the reduction of available space on the chambers promote the reduction of volume used in reagents and sample, performing the immunoassay protocol with minimum resources. From the bottom to the top, the first layer (Acetate) contains the inlets for the electrolysis pumps and holes for the glassy carbon connections. The second layer (PSA) has the microchannels that connect

Parameter	Value	Parameter	Value
ρ	997 kg/m^3	F	96480 $Cmol^{-1}$
P_{atm}	101325 Pa	T_{EP}	293.15 K
R	8.3145 $m^3Pamol^{-1}K^{-1}$	V_0 (electrolysis pump)	5.69 $\times 10^{-8}m^3$
Cross-sectional Area (siphon channel)	3 $\times 10^{-8}m^2$	T_0	296.15 K
T	348.15 K	r_m	5 mm
j	200 μm	V_0 (RTP Valve)	2 $\times 10^{-7}m^3$

Table 4.1: **Parameters used to design and model the electrolysis pump.**

the electrolysis chambers to the sample chambers (washing, reagents chambers) and channels that interconnect the double electrolysis pumps. The third layer (PC) has all the chambers engraved. The fourth layer (PSA) shares almost the same design than the previous layer, but contains the siphon channel from the washing chambers to the detection chamber and the main microchannel of the CD. From the fifth to the eighth layer, it is cut the parts to form the 3D siphon channel connecting the reagent chambers with the main microchannel. The last layer (Acetate) contain the holes to permit the contact of the GC electrodes with the electrolysis chambers and the inlets for the majority of the chambers.

To reduce the amount of layers in the Phase 4 CD, the RTPV valve is added externally by assembling it square by square above of the last layer. The electrolysis chambers in the Phase 3 and 4 CDs are sealed by pasting the GC electrode substrate using double PSA. The **Figure 4.5** shows photos of the CDs assembled.

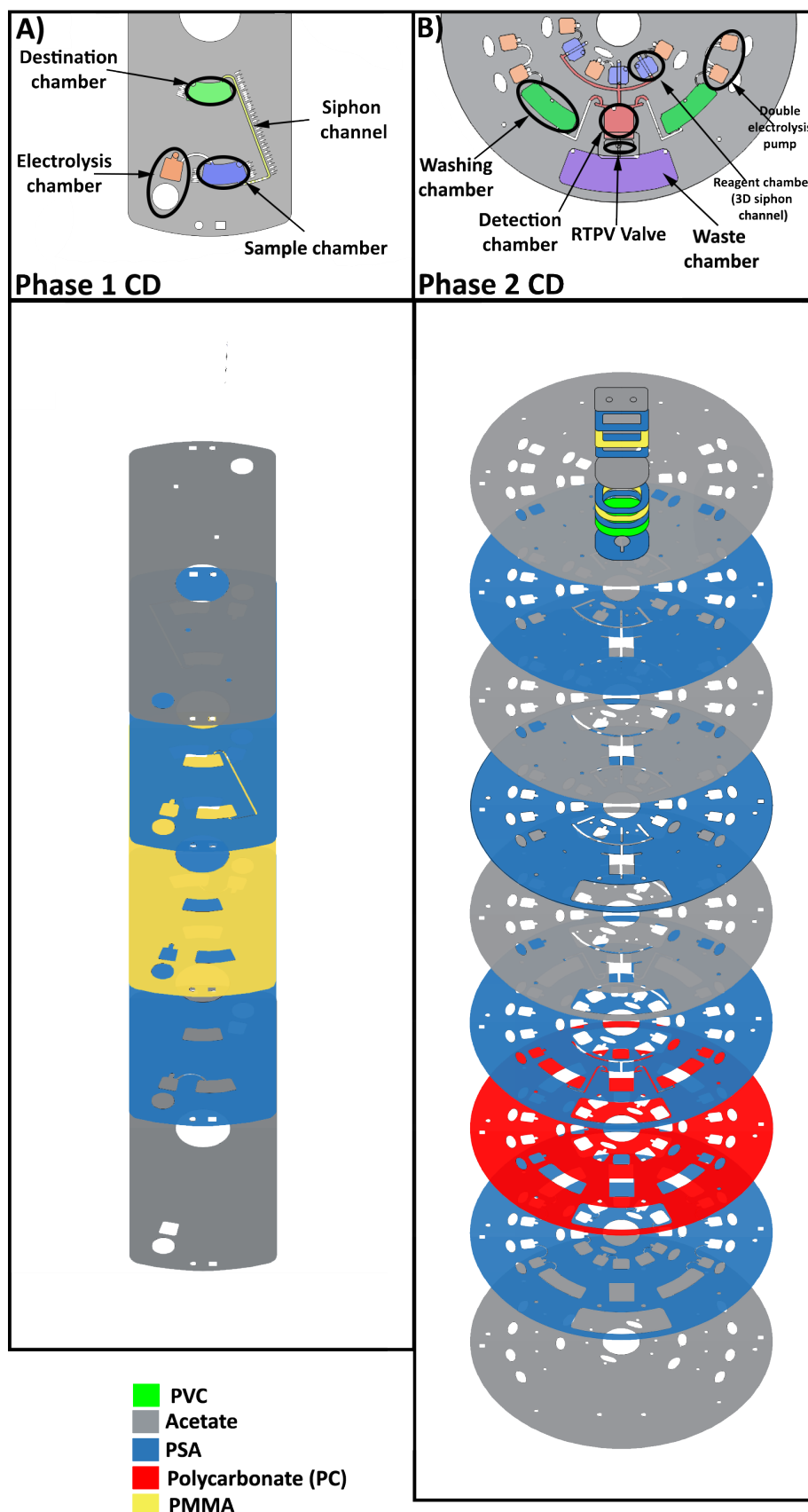


Figure 4.4: *Design and layers of the CD developed for the characterization of the wireless electrolysis pump and the automation of immunoassay.*

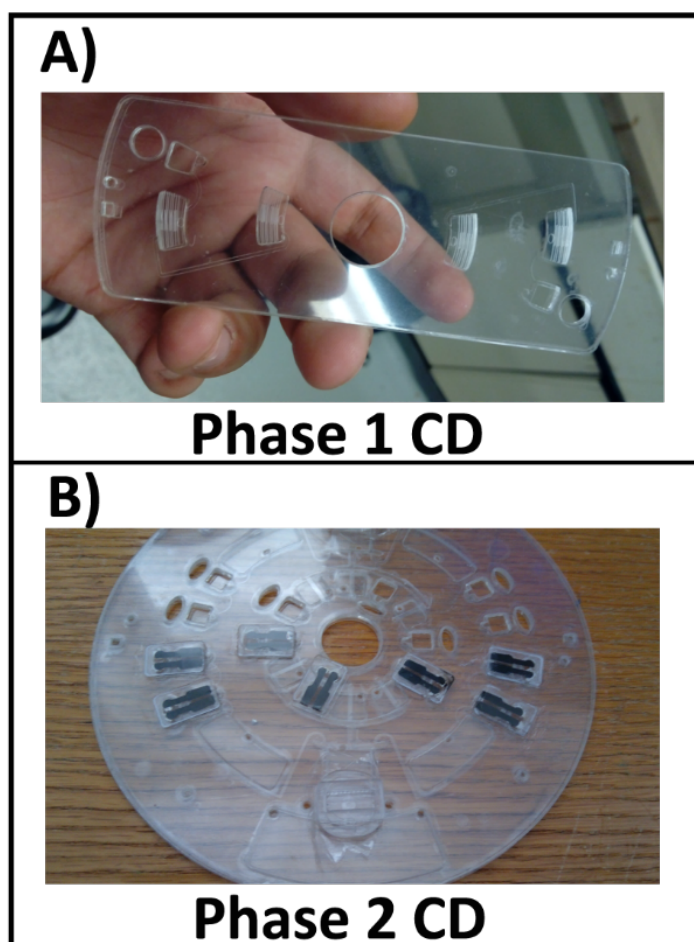


Figure 4.5: *Photos of CDs used for the characterization of the wireless electrolysis pump (Phase 1) and the automation of immunoassay (Phase 2).*

4.3 eLoaD implementation: electrical circuit and mobile application design

The eLoaD circuit is required to electrically supply the electrolysis pumps and RTPV inserted on the CD. However, the eLoaD is only an Arduino cartridge which requires to be complemented with a personalized PCB circuit with all the required elements for the actuators. As well, the eLoaD board proportionate Bluetooth communication for data transfer to either a computer or a smartphone. The development of an android application was required to enable the wireless control of the pumps and valve for the user. The PCB-Android application was designed for the phase 2 CD. The **Figure 4.6** illustrates two block diagrams, each of them explaining the general operation of the

android application and PCB logic.

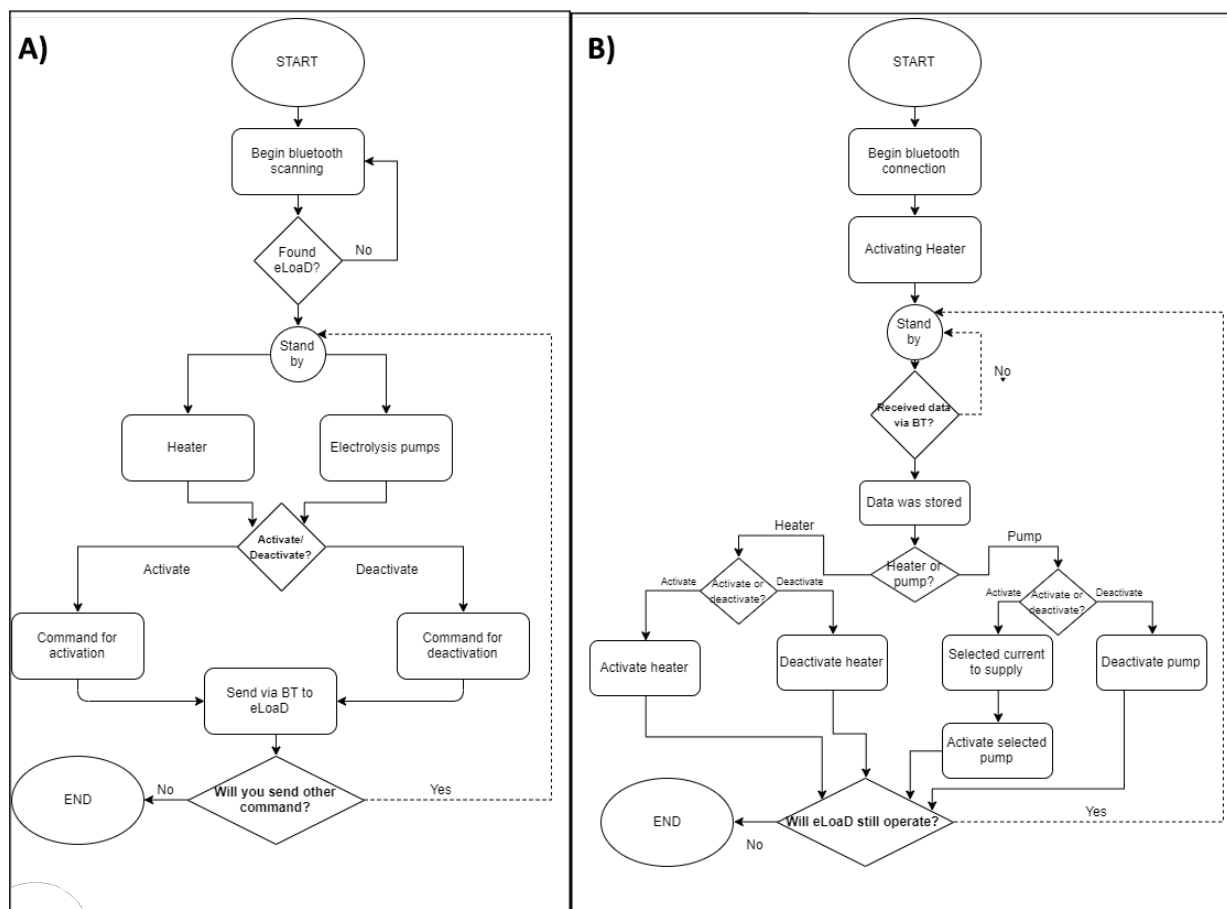


Figure 4.6: *Block diagrams of the general operation of the android application and eLoaD circuit united with the PCB. A) After being coupled with the eLoaD, the application waits for the user input related to the manipulation of the heater (RTPV) or the electrolysis pump. The application sends the corresponding command to activate or deactivate either of the actuators to the eLoaD. B) The eLoaD is in stand-by until the Bluetooth communication receives data. The Arduino code on the eLoaD interprets the data to select the activation or deactivation of a determined electrolysis pump or the heater in the valve. The circuit can manipulate the electrical current magnitude to send to the pumps.*

Development of Android application

The development of a tool that permit simplify the control of the steps on the CD by activating different actuators instead of depending the change of spinning velocity in the platform to continue the protocol. For this purpose, an android application was developed that enables the command transfer to the eLoaD circuit via Bluetooth. The app (**Figure 4.7**) enables the activation or deactivation of seven electrolysis pumps and the heater of the RTPV valve simultaneously. The app sends "+=" command, where "+" represents "v" for the heater and "p" for the pump; "=" can be a range of number from 0 to 8. For the heater control, "1" activates it and "2" deactivates it. For the selection of pumps, by sending a value from "1" to "7" the user can activate the corresponding pump on the CD and "8" deactivates the current pump. Both applications were programmed using the tool "MIT App inventor" webpage (MIT, MA, USA). The block programming generated for the application can be consulted in the section **Appendix B**.

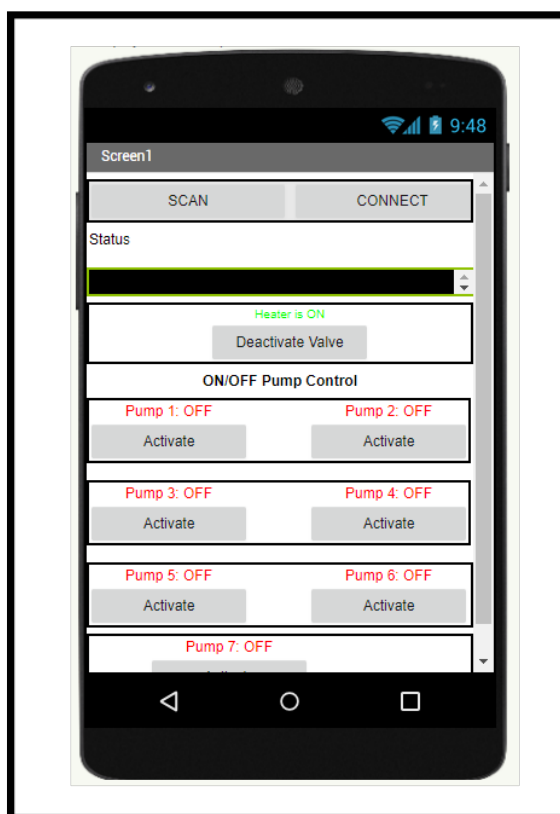


Figure 4.7: *The mobile application developed for wireless control of electrolysis pumps and RTPV valves on CDs integrated with an eLoaD.*

Electrical circuit design and fabrication

As it has been mentioned previously, the electrical circuit has to accomplish two

tasks: 1) Provide electrical current to the electrodes to initiate the electrolysis reaction for pumping and 2) supply adequate voltage to actuate an electrical resistor/heater for RTPV valving. The PCB circuit was designed using the software Diptrace (Novarm Ltd., Dnipropetrovsk, Ukraine) and fabricated by the company MillerSanchez, Mexico. A current control module was added for the electrodes because the flow rate generated by the electrolysis pump (**Eq. 3.22**) can be predicted in terms of electrical current instead of voltage. To supply enough power to generate heat, the resistor was connected serially with a MOSFET transistor (BSS138P) to maintain a stable current from the microcontroller. The modules used for the PCB circuit for the electrolysis pump control is structured in three parts:

- **Digital-to-Analog Converter (DAC) module.** The DAC module can generate an output voltage magnitude depending of the two bytes that are send by the Arduino. In consequence of, this module can modified the electrical current value that the electrolysis pump will received (by the relation voltage-current explained in the Ohm's law $V = RI$).
- **Voltage-to-Current Converter (VCC) module.** The voltage sent by the DAC module arrives to the VCC module which will convert it to electrical current that passes through the electrolysis pumps connected in the feedback loop of the Operational Amplifier (OpAmp). This feedback loop in the OpAmp maintains the electrical current in constant values until the resistance generated in the electrolysis pumps increases. A simulation of this module done in LtSpice 17 (Analog Devices, MA, USA) shows the range of current available for the pumps by using the OpAmp *OP777* (See more in **Appendix A**).
- **Selector of pump (Demultiplexer).** The demultiplexer connected between the electrolysis pumps and the VCC module enables to select to which pump we require to create continuity with the OpAmp, letting the activation of electrolysis.

The **Figure 4.8** shows photos of the fabricated PCB board. The circuit schematic used for the PCB board can be consulted in **Appendix A**.

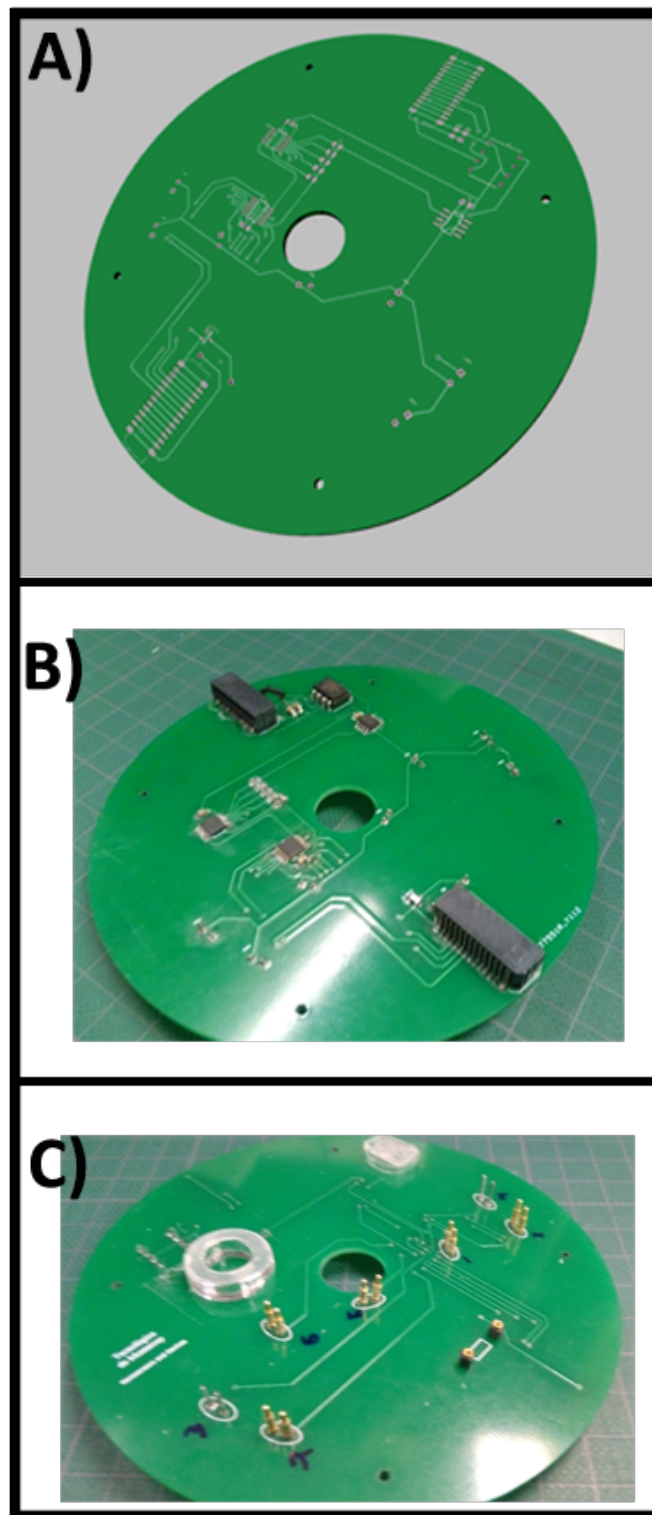


Figure 4.8: *Photos and illustration of the PCB board for Phase 2 CD. A) Illustration obtained in Diptrace emulating the copper pathways in top view. B) Photos (Top and Bottom view) of the fabricated PCB board.*

4.4 Glassy carbon electrodes fabrication

Glassy carbon is an inexpensive, easy to fabricate, inert and bio-compatible material and therefore was selected for the fabrication of electrodes for electrolysis pumping. Using these electrodes can assure that during the electrolysis reaction there will not be generated oxides that can contaminate the test.

The glassy carbon electrodes were fabricated from pyrolyzation of SU-8 2025 (MicroChem, MA, USA) polymer precursor. The fabrication is divided in two process: photolithography and pyrolysis. The photolithography starts by spin coating the photoresist on silicon (University wafer, MA, USA) and $500\mu\text{m}$ fused silica (University wafer, MA, USA) at 4000 RPM for 30 seconds, to a final layer thickness of $20\mu\text{m}$. The soft-bake was done for 5 minutes at 95°C to evaporate solvents. The photoresist was exposed to UV radiation through a photomask to a total energy of $120\text{mJ}/\text{cm}^2$. Then, the sample was soft-baked once again for 5 minutes at 95°C to finish the cross-link reaction. Finally, the unexposed regions were dissolved in SU-8 developer (MicroChem, MA, USA) by immersing it during 3 minutes.

The samples were pyrolyzed in a pressured furnace PEO-601 (ATV Technologie GmbH, Germany) with ultra-pure nitrogen environment (5 l per min) using the next temperature profile proposed by Pramanick et al.[64] (**Figure 4.10.A**): 1) The temperature increases from room temperature to 300°C with $5^\circ\text{C}/\text{min}$ as temperature ramp rate and maintained during 60 min. 2) The temperature increases from 300°C to 900°C with the same ramp rate and maintained during 60 min. 3) Finally, the furnace was cooled down to room temperature. The **Figure 4.10.B-E** shows photos of the electrodes after the pyrolysis on the quartz tube and in different substrates. The resistance on the GC electrodes was measured using a digital multimeter MUT-33 (Truper, Mexico), getting a value range from 50 to $120\ \Omega$. The electrodes on fused silica substrate were cut by the laser CNC model STM-L1390B (STM Robotics, Mexico).

4.5 Experimental setup and procedure

A custom made experimental setup has been used to test all the CDs presented on this section. The setup integrates a servo motor model J0100-303-3-000 (Applied motions, CA, USA) controlled by a motor driver SV7-S-AE (Applied motions, CA, USA). A transmitter coil is set in the top of the motor to supply power wirelessly to the eLoad (wielded a receiver coil). The **Figure 4.11.A** is a describing configuration of the eLoad parts positioned in the spinning motor. The image acquisition was performed using a high-speed camera X10 zoom (Imaging source, NC, USA) and a stroboscope SHIMPO

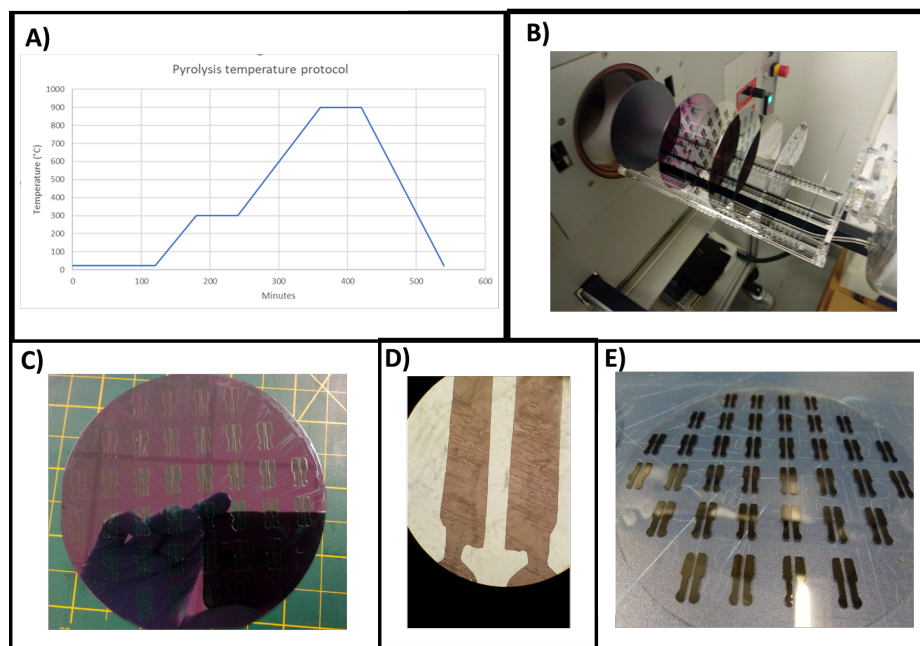


Figure 4.9: *Illustrations about the process of pyrolysis step for GC electrodes. A) Temperature protocol used during the pyrolysis process. B) Photo of quartz tube with the samples after pyrolysis. C) Photo of 20 μ m height GC electrodes on silicon substrate. D) Photo using a microscope showing the carbon pattern in the electrodes. E) Photo of 20 μ m height GC electrodes on fused silica substrate.*

model DT-311A (Shimpo, NY, USA). All the equipment was controlled in sync by a LabView program (National Instruments, TX, USA). The electrical supply during the flow rate measurements was performed by a 6-slip ring/brush assembly model 0906 (Fabricast, CA, USA). The **Figure 4.11.B** illustrates the complete equipment setup used for the tests.

Characterization of flow rate: Phase 1 CD

The phase 1 CD was used to measure the flow rate generated by the electrolysis pump while using GC electrodes in the electrolysis chamber. 35 μ L of 0.8 M aqueous solution of sodium sulfate and 60 μ L of colored water were filled in the electrolysis and sample chamber respectively. The experiment was recorded in two variations: The flow rate generated on constant electrical current (2 mA) in a range of 600 to 1500 RPM and the flow rate generated on constant rotational speed (1200 RPM) in a range of 1 to 5 mA. The multiple videos were analyzed using the "image processing" toolbox on MATLAB R2018a (Mathworks, MA, USA) to measure the changes of liquid level in the sample chamber and siphon channel. The MATLAB code used for this analysis can be checked on **Appendix B**.

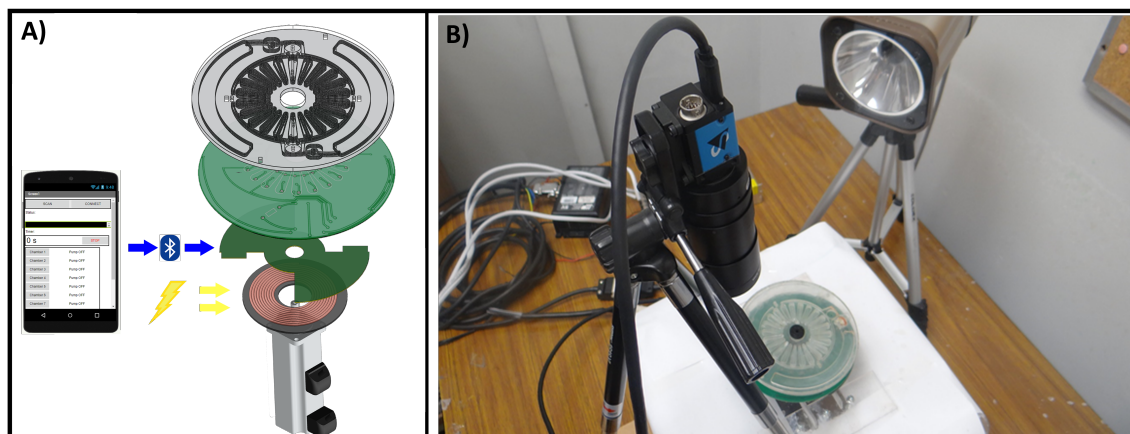


Figure 4.10: *Experimental setup for the multiple studying CD platforms developed in this work. A) The configuration of the eLoaD parts and the CD platform connected to BT. B) Photo of the spin-stand used for the CD microfluidic experiments.*

Automated immunoassay based on peptides microarray:Phase 2 CD

As an application, the phase 2 CD was designed to adapt the immunoassay based on peptides microarray. To demonstrate that the electrolysis pumps can mobilize small volumes of reagents in a strict order, the amount of volume used for each reagent/sample corresponds to the displaced volume in the phase 1 CD. The phase 2 CD design was optimized to reduce the amount of plastic layers in comparison to the platform seen in [42] and **Appendix A**. The footprint in the platform has been reduced by providing one chamber for the washing buffer which is the reagent used in multiple times in the assay. The buffer transference can be cut by stopping the pumping actuation, maintaining the rest of the volume in the destination chamber without suffering leakage. The configuration of electrolysis pumps and RTPV provides a complete automation for the CD platform.

The **Figure 4.11** displays the order of steps in the CD assay to use the first two reagents in the test (Washing and blocking buffer). The peptides microarray, provided by Pepperprint, contained 800 peptides per cm which they were 5 peptides: monoclonal anti- Hemagglutinin (HA), anti-Flag antibodies, polio virus, Tetanus and *S. aureus*. The glass slide (1cmx1cm), where the microarray is fixed, has been placed in the detection chamber. As a first detection, the HA antibodies were chosen because of detection equipment limitations.

The washing chambers were filled with 150 μL of PBS-T (1 x PBS, Sigma Aldrich, pH 7.4, 0.05% v/v Tween 20, Sigma Aldrich), the blocking chamber with 50 μL of

Rockland blocking buffer, the sample chamber with 50 μL of serum diluted 1:500 in PBS-T with 10% v/v blocking buffer and secondary antibodies chamber with 50 μL of AF647 conjugated anti-human IgG (Fc) antibodies (Jackson ImmunoResearch, West Grove, PA, USA) diluted to 0.25 $\mu\text{g mL}^{-1}$ in PBS-T with 10% v/v blocking buffer (For the test, the mixture contained monoclonal AF488 conjugated anti-HA antibodies diluted to 1 $\mu\text{g mL}^{-1}$). The test started with spinning up the CD to 600 RPM (**Figure 4.11.A**) and then activating the electrolysis pump in the washing chamber to inject 50 μL washing solution to the detection chamber (**Figure 4.11.B**) to clean the microarray area from contaminants. The pump stopped and the buffer incubated in the chamber for 10 minutes (**Figure 4.11.C**). Then, the RTPV heater was turned off to move the used buffer to the waste chamber (**Figure 4.11.D**). The RTPV was turned on once again and the electrolysis pump connected to the blocking chamber was activated, moving the buffer to the detection chamber to block the adhesion of the sample to the unfunctionalized surface, reducing the noise signal in the following detection (**Figure 4.11.E**). The electrolysis pump was deactivated and the blocking buffer was incubated for 30 minutes and then the valve was also deactivated to move the liquid to the waste chamber afterwards (**Figure 4.11.F-G**). The detection chamber was filled with 50 μL of washing buffer once again and incubated for 10 minutes (**Figure 4.11.H**). The serum sample was transferred to the detection chamber and incubated for 1 hour. Afterwards, the chamber was washed twice and the secondary antibody solution was introduced and incubated over the peptide array on the detection chamber for 1 hour. The last two washing steps were performed, each for 10 seconds in the incubation. In parallel to this test, a second peptides microarray was incubated on a rotational shaker with 140 RPM as a control test.

The microarrays were cleaned with deionized water and dried with argon gas. Both microarrays were analyzed by fluorescence with the scanner "Odyssey Infrared Imaging System" (LI-COR, NE, USA, 680 nm and 800 nm). The fluorescence intensity was analyzed with the PepSlide Analyzer software (Sicasys, GmbH, Germany), calculating the median intensity on 171 peptide spots corresponding to the HA antibody.

Peptides microarray protocol: First steps

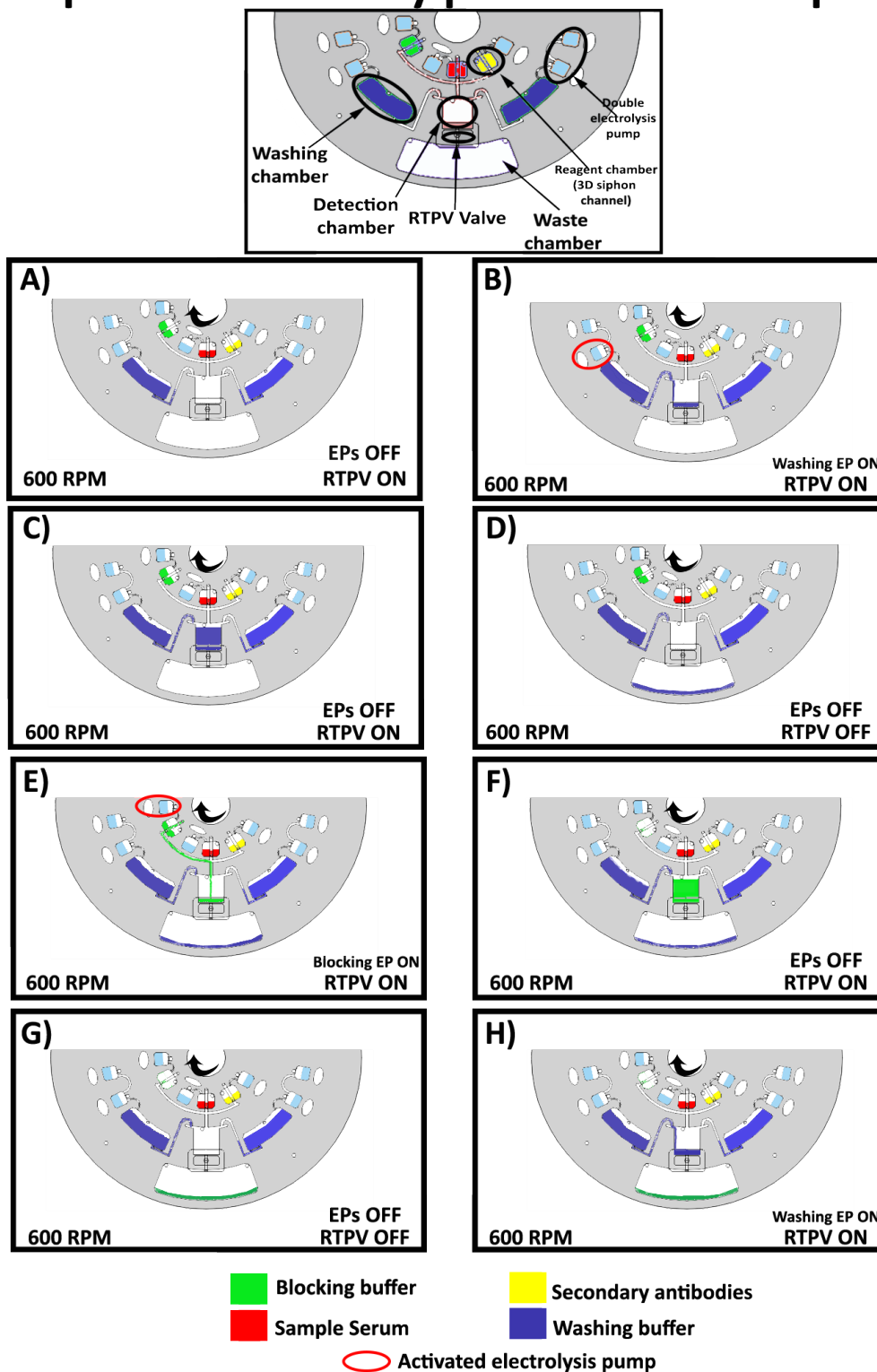


Figure 4.11: *Schematic illustration of the performance of Phase 2 CD in peptides microarray test. The schematic shows the steps for the first two reagents (Washing and blocking buffer) travelling through the platform.*

Chapter 5

Results and Discussion

This chapter evaluates the results obtained from the experimental procedure demonstrated in the chapter 4 **Materials and methods**. The data obtained from the "phase 1 CD" are used to determine the range of flow rate the wireless electrolysis pump provides by using as low electrical current as 1 to 5 mA. The experiments in the second phase of the study is a demonstration of the practicality of the wireless electrolysis pumps for the automation of complex immunoassays.

5.1 Flow rate characterization during pumping regime

Previous to the flow rate measurement, it was required to know the maximum electrical current that the glassy carbon electrodes (see more in **Materials and methods**) can provide to the pump. Multiple electrodes embedded to the phase 1 CD were tested (**Figure 4.4.A**) to measure the electrical current with a multimeter MUT-33 (Truper, Mexico). The maximum electrical current that the glassy carbon can manage for water electrolysis is 5 mA while providing 10 V to the electrical cell. Knowing the electrical limits, the flow rate analysis was established under the current range of 1 to 5 mA and rotational velocity from 600 RPM to 1500 RPM. This velocity range was established by comparing the rotational velocity profile used on previous works [14, 33, 35, 36, 37, 39, 40, 42, 51, 53]. The **Figure 5.1** shows the pneumatic pressure (**Eq. 3.20**) required to move $60\mu L$ while applying different rotational velocities. The electrolysis pump is modeled with the assumption that the pneumatic pressure generated by the gases can overcome the centrifugal pressure (**Eq. 3.2**) which is dependent to the rotational speed. The graph highlights the presence of the two regimes during the pumping: The transient regime where the pneumatic pressure increases rapidly but the volume displacement is

small (**Figure 5.1.A-B**), and the steady-state regime at which the pneumatic pressure increases slowly but the volume displacement is increases rapidly (**Figure 5.1.C-E**). The pneumatic pressure was calculated using the **Eq.3.20** by the change of distance of meniscus in the sample chamber and siphon channel. The **Figure 5.1** has shown that the amount of liquid moved during the transient regime is very small (1.167%) in comparison to the steady-state one. The last statement needs to be considered when the pump is integrated in a precise assay because the existence of a transient flow rate is equivalent to a small offset volume delivered to the destination.

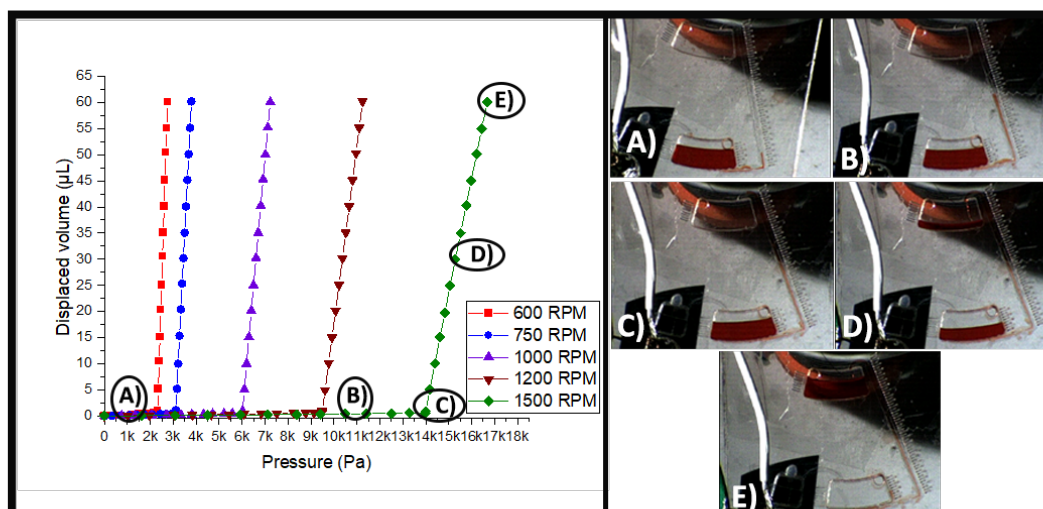


Figure 5.1: *Pneumatic pressure required to move liquid volume by electrolysis pump at different rotational speeds. Between A) and C) the pumping performance is ruled by the transient regime (filling of siphon channel) while C) to E) present a steady-state regime. E) The entire volume fills the destination chamber.*

The **Figure 5.2** displays the flow rate calculated by the variation of rotational velocity while applying constant current (2 mA); the flow rate in the transient and steady-state regime were calculated separately. The decreasing behavior in both regimes confirms that the flow rate is inversely proportional to the square of the angular velocity according with the mathematical model developed by Noroozi et al. [31] (**Eq.3.22**) . The theoretical flow rate was higher than the experimental values, however this behavior was constant in all the measurements. By applying a correction factor of **0.582** to the theoretical data, both flow rates have similar values through the velocities used. By increasing the velocity from 600 to 1500 RPM , the flow rate is from 0.127 to 0.234 $\mu\text{L}/\text{s}$.

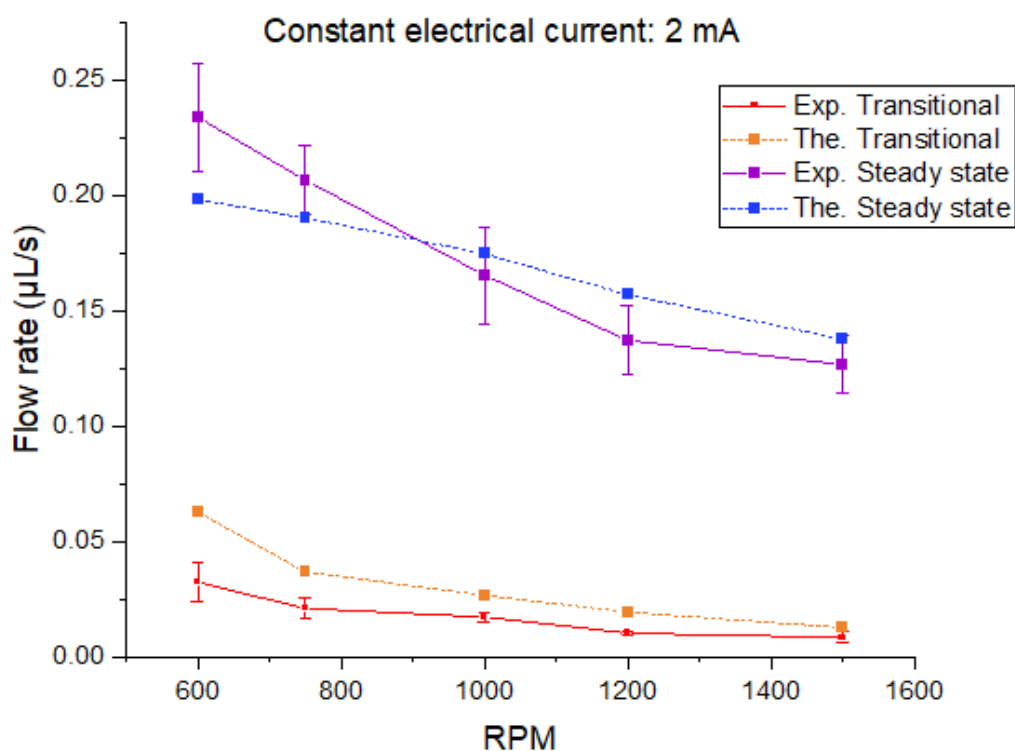


Figure 5.2: *Experimental and theoretical analysis of carbon electrolysis pumping flow rate while increasing the rotational speed.*

The **Figure 5.3** displays the flow rate calculated by the variation of electrical current on a constant rotational speed (1200 RPM). Similar to the previous figure, the flow rate is divided by the two existing regimes (transient and steady-state). The theoretical data has been corrected using the same factor of **0.582**, as the case of flow rate-rotational speed. The theoretical and experimental flow rate have an increasing linear behavior and the flow rate is proportional to the electrical current according with **Eq.3.22**. The flow rate changes from 0.0711 to 0.4311 $\mu L/s$. The flow rate range generated by changing the electrical current is wider in comparison to the one generated by changes of rotational speed. By the previous statement, we reached to two conclusions: To achieve the movement of liquid volume on nanoscale it is required to supply the pump with a very low current and to deliver thereagents on different flow rates it is recommended to change the current instead of the rotational speed. By not adding more changes of rotational speed, the velocity profile required to actuate the assay on CD can be simplified.

The conventional electrolysis pump on CD platform [31] enabled the manipulation of a wide range of flow rate from 0.5 to 8 $\mu L/s$. However, the pump required a high current (90 mA) and therefore coupling the electrodes with a specialized power supply (slip ring) that's expensive, noisy, bulky and limited to a determined number of connections, reducing the implementation of the system on POC setting.

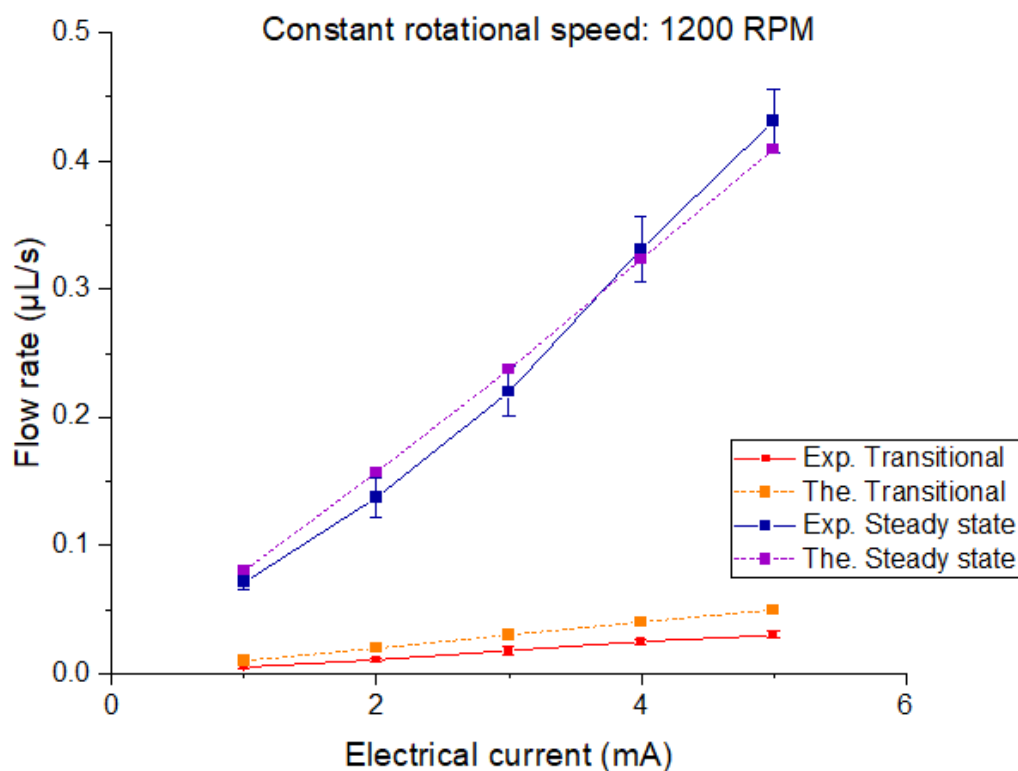


Figure 5.3: *Experimental and theoretical analysis of electrolysis pumping flow rate at different electrical current.*

5.2 Peptides microarray protocol on CD platform

The **Figure 5.4** shows the fluorescence scan of the control peptides microarray (left side), which was incubated following the standard protocol on petri dish, and the CD peptides microarray (right side) and their average fluorescence intensities respectively. By comparing the results obtained by Aeinehvand et al. [42], the present study changes some factors: The reduction of reagent and sample volumes from $400\mu\text{L}$ to $50\mu\text{L}$ and the elimination of shaking sections. Previously on **Materials and methods**, the reduction of volumes was justified because of the displaced volumes used during the phase 1; this entire volume covers completely the glass slide surface which we expected to assure a decent immunocapture in all the peptides array. We eliminated the shaking steps on the assay as covering the surface with the volumes was enough to achieve a positive response in the fluorescence detection. However, the low intensity detected demonstrates that the integration of a mixing technique is crucial to assure a better capture on the microarray, even if the CD platform will not be running in one rotational speed (600 RPM). In the cases that the fluorescence intensity must be equal to the one

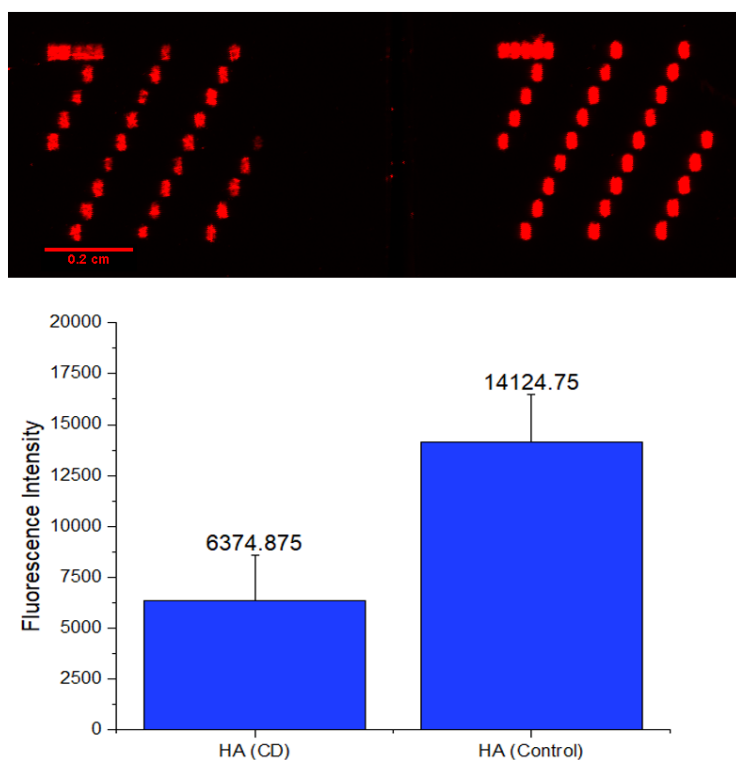


Figure 5.4: *Fluorescence scans of control and CD peptides microarrays and their average intensities.*

obtained by following a standard immunoassay protocol, it is recommended to add the shaking steps in each incubation interval (These steps will not be problematic for the electrolysis pump performance). During the immunoassay testing, the electronic circuit delivered a decreasing electrical current as the electrolysis pump was still on for long amount of time]. By testing separately the glassy carbon electrodes in an electrolysis reaction, their surface showed a brighter surface color and became more brittle. The previous statement is related to the increase of resistance by the electrodes which causes a less efficient current transference.

Chapter 6

Conclusions and future work

This chapter presents a general conclusion derived by the design, fabrication and testing of the centrifugal microfluidic systems for the optimization of the wirelessly controlled electrolysis pump and automated immunoassay. Moreover, this chapter includes suggestions for future work and improvements on the CD system, specially real-life POC presented.

6.1 Conclusions

This work has demonstrated the integration of multiple electrolysis pumps can enable the mobilization of the reagents independent to each other by control of the user. The electrolysis pump with integrated glassy carbon electrodes can deliver small liquid volumes (max. $60 \mu L$) in a flow rate range from 0.0711 to $0.4311 \mu L/s$. The previous parameters were enough to apply this kind of pump to a detection technique on CD such as peptides microarray based immunoassay. The positive response by HA antibody during the CD assay proved the efficiency of the pumps to the reagents without disturbing the test. For further assays, the implementation of a mixing technique to increase the intensity response is expected.

Even if the electrical current offered by the eLoaD platform is 18 times lower than that of slip ring used in conventional electrolysis pump, the low flow rate induced by the wireless setup enables a precise liquid control in nano-scale. The liquid control on nano-scale can be employed for more sensible detection assays because the continuous liquid transfer offered by the pump. Even if the use of active actuators such as heaters or the electrolysis pump required to add extra equipment (as the case of the eLoaD board and its inductors for power supply), the electronic system presented on this work compensates the same actuation done by power supplies with limited connections [31] and bulky mechanical actuators [39,54]. An advantage of the use of the electrolysis

pump is the reversible actuation that offers; by stopping the pumping actuation, the liquid volume stored in its chamber will not generate leakage in comparison to the sacrificial valves which have an “all or nothing” behavior [14,35,40,50,51]. The reversible behavior on the electrolysis pump enables the “metering” feature, meaning that the entire liquid inside of a chamber can be delivered in fixed volumes. Another advantage of the electrolysis pump is that it can be actuated independent to the changes of centrifugal pressure, where it does not require a burst frequency in comparison to valves actuated by this way [33, 37, 42]. Finally, the flow rate on nano-scale created by the pump opens to the possibility to explore the use of very low liquid volume.

The manipulation of steps by the user and the easy redesign of the pump are some advantages that promoted their adaptation in other bioassays such as Polymerase chain reaction (PCR) and Loop-mediated isothermal amplification (LAMP). Because of the precise low flow rate, the adaptation of the electrolysis pump to generate droplets on CD platforms is another option for further work.

6.2 Future work

To demonstrate the multiplexing feature on the peptides microarray, a more complete immunoassay on the CD will be implemented for the next targets: FLAG and HA antibodies, Polio, Tetanus and *S. aureus*. This test will prove the efficiency of the system to detect multiple diseases on a POC setting.

The PCB circuit on this work will be modified to extend the electrical current range available for the pump and assure its optimal performance for longer interval of time.

Chapter 7

Bibliography

- [1] H. Pasquini-descomps, N. Brender, and D. Maradan, “Value for Money in H1N1 In fl uenza : A Systematic Review of the Cost-Effectiveness of Pandemic Interventions,” *Value in Health*, vol. 20, no. 6, pp. 819–827, 2017.
- [2] A. Galindo-Fraga, A. A. Ortiz-Hernández, A. Ramírez-Venegas, R. V. Vázquez, S. Moreno-Espinosa, B. Llamosas-Gallardo, S. Pérez-Patrigeon, M. Salinger, L. Freimanis, C. yu Huang, W. Gu, M. L. Guerrero, J. Beigel, and G. M. Ruiz-Palacios, “Clinical characteristics and outcomes of influenza and other influenza-like illnesses in Mexico City,” *International Journal of Infectious Diseases*, vol. 17, no. 7, pp. 19–21, 2013.
- [3] G. Soto-Estrada, L. Moreno-Altamirano, D. Pahua Díaz, G. Soto-Estrada, L. Moreno-Altamirano, and D. Pahua Díaz, “Epidemiological overview of Mexico’s leading causes of morbidity and mortality,” *Revista de la Facultad de Medicina (México)*, vol. 59, no. 6, pp. 8–22, 2016.
- [4] S. de salud, “Dirección General de Epidemiología Anuario de Morbilidad 1984 - 2018,” 2018.
- [5] World Health Organization, “Capital health expenditure,” 2019.
- [6] M. Urdea, L. A. Penny, S. S. Olmsted, M. Y. Giovanni, P. Kaspar, A. Shepherd, P. Wilson, C. A. Dahl, S. Buchsbaum, G. Moeller, and D. C. Hay Burgess, “Requirements for high impact diagnostics in the developing world,” *Nature*, vol. 444, p. 73, nov 2006.
- [7] J. Gilmore, M. Islam, and R. Martinez-Duarte, “Challenges in the use of compact disc-based centrifugal microfluidics for healthcare diagnostics at the extreme point of care,” *Micromachines*, vol. 7, no. 4, 2016.

- [8] V. Gubala, L. F. Harris, A. J. Ricco, M. X. Tan, and D. E. Williams, “Point of care diagnostics: Status and future,” *Analytical Chemistry*, vol. 84, no. 2, pp. 487–515, 2012.
- [9] A. M. Foudeh, T. Fatanat Didar, T. Veres, and M. Tabrizian, “Microfluidic designs and techniques using lab-on-a-chip devices for pathogen detection for point-of-care diagnostics,” *Lab on a Chip*, vol. 12, no. 18, pp. 3249–3266, 2012.
- [10] W. Su, X. Gao, L. Jiang, and J. Qin, “Microfluidic platform towards point-of-care diagnostics in infectious diseases,” *Journal of Chromatography A*, vol. 1377, pp. 13–26, 2015.
- [11] C. W. Tsao, “Polymer microfluidics: Simple, low-cost fabrication process bridging academic lab research to commercialized production,” *Micromachines*, vol. 7, no. 12, 2016.
- [12] M. Madou, J. Zoval, G. Jia, H. Kido, J. Kim, and N. Kim, “Lab on a Cd,” *Annual Review of Biomedical Engineering*, vol. 8, no. 1, pp. 601–628, 2006.
- [13] L. X. Kong, A. Perebikovskiy, J. Moebius, L. Kulinsky, and M. Madou, “Lab-on-a-CD: A Fully Integrated Molecular Diagnostic System,” *Journal of Laboratory Automation*, vol. 21, no. 3, pp. 323–355, 2016.
- [14] T. H. Kim, K. Abi-Samra, V. Sunkara, D. K. Park, M. Amasia, N. Kim, J. Kim, H. Kim, M. Madou, and Y. K. Cho, “Flow-enhanced electrochemical immunosensors on centrifugal microfluidic platforms,” *Lab on a Chip*, vol. 13, no. 18, pp. 3747–3754, 2013.
- [15] C. Yi, Q. Zhang, C. W. Li, J. Yang, J. Zhao, and M. Yang, “Optical and electrochemical detection techniques for cell-based microfluidic systems,” *Analytical and Bioanalytical Chemistry*, vol. 384, no. 6, pp. 1259–1268, 2006.
- [16] X. Duburcq, C. Olivier, F. Malingue, R. Desmet, A. Bouzidi, F. Zhou, C. Auriault, H. Gras-Masse, and O. Melnyk, “Peptide-Protein Microarrays for the Simultaneous Detection of Pathogen Infections,” *Bioconjugate Chemistry*, vol. 15, no. 2, pp. 307–316, 2004.
- [17] L. C. Szymczak, H. Y. Kuo, and M. Mrksich, “Peptide Arrays: Development and Application,” *Analytical Chemistry*, vol. 90, no. 1, pp. 266–282, 2018.
- [18] M. Cretich, F. Damin, G. Pirri, and M. Chiari, “Protein and peptide arrays: Recent trends and new directions,” *Biomolecular Engineering*, vol. 23, no. 2-3, pp. 77–88, 2006.

- [19] C. Lui, S. Stelick, N. Cady, and C. Batt, “Low-power microfluidic electro-hydraulic pump (EHP),” *Lab on a Chip*, vol. 10, no. 1, pp. 74–79, 2010.
- [20] D. N. Pagonis, A. Petropoulos, and G. Kaltsas, “A pumping actuator implemented on a PCB substrate by employing water electrolysis,” *Microelectronic Engineering*, vol. 95, pp. 65–70, 2012.
- [21] H. Kim, H. Hwang, S. Baek, and D. Kim, “Design, fabrication and performance evaluation of a printed-circuit-board microfluidic electrolytic pump for lab-on-a-chip devices,” *Sensors and Actuators, A: Physical*, vol. 277, pp. 73–84, 2018.
- [22] Y. Yi, U. Buttner, A. A. Carreno, D. Conchouso, and I. G. Foulds, “A pulsed mode electrolytic drug delivery device,” *Journal of Micromechanics and Microengineering*, vol. 25, no. 10, 2015.
- [23] Y. Yi, A. Zaher, O. Yassine, J. Kosel, and I. G. Foulds, “A remotely operated drug delivery system with an electrolytic pump and a thermo-responsive valve,” *Biomicrofluidics*, vol. 9, no. 5, pp. 1–9, 2015.
- [24] Y. Yi, U. Buttner, and I. G. Foulds, “A cyclically actuated electrolytic drug delivery device,” *Lab on a Chip*, vol. 15, no. 17, pp. 3540–3548, 2015.
- [25] P. Y. Li, J. Shih, R. Lo, S. Saati, R. Agrawal, M. S. Humayun, Y. C. Tai, and E. Meng, “An electrochemical intraocular drug delivery device,” *Sensors and Actuators, A: Physical*, vol. 143, no. 1, pp. 41–48, 2008.
- [26] R. Sheybani and E. Meng, “High efficiency wireless electrochemical actuators: Design, fabrication and characterization by electrochemical impedance spectroscopy,” *Proceedings of the IEEE International Conference on Micro Electro Mechanical Systems (MEMS)*, pp. 1233–1236, 2011.
- [27] H. Gensler, R. Sheybani, P. Y. Li, R. Lo, S. Zhu, K. T. Yong, I. Roy, P. N. Prasad, R. Masood, U. K. Sinha, and E. Meng, “Implantable MEMS drug delivery device for cancer radiation reduction,” *Proceedings of the IEEE International Conference on Micro Electro Mechanical Systems (MEMS)*, no. Di, pp. 23–26, 2010.
- [28] J. Sim, D. S. Kwon, and J. Kim, “Acid-sensitive pH sensor using electrolysis and a microfluidic channel for read-out amplification,” *RSC Advances*, vol. 4, no. 75, pp. 39634–39638, 2014.
- [29] X. Li, D. Li, X. Liu, and H. Chang, “Ultra-monodisperse droplet formation using PMMA microchannels integrated with low-pulsation electrolysis micropumps,” *Sensors and Actuators, B: Chemical*, vol. 229, pp. 466–475, 2016.

- [30] J. C. Kuo, P. H. Kuo, H. T. Hsueh, C. W. Ma, C. T. Lin, S. S. Lu, and Y. J. Yang, “A capacitive immunosensor using on-chip electrolytic pumping and magnetic washing techniques for point-of-care applications,” *Proceedings of the IEEE International Conference on Micro Electro Mechanical Systems (MEMS)*, pp. 809–812, 2014.
- [31] Z. Noroozi, H. Kido, and M. J. Madou, “Electrolysis-Induced Pneumatic Pressure for Control of Liquids in a Centrifugal System,” *Journal of The Electrochemical Society*, vol. 158, no. 11, p. P130, 2011.
- [32] Z. Noroozi, H. Kido, R. Peytavi, R. Nakajima-Sasaki, A. Jasinskas, M. Micic, P. L. Felgner, and M. J. Madou, “A multiplexed immunoassay system based upon reciprocating centrifugal microfluidics,” *Review of Scientific Instruments*, vol. 82, no. 6, pp. 1–9, 2011.
- [33] Y. Ukita, S. Kondo, T. Azeta, M. Ishizawa, C. Kataoka, M. Takeo, and Y. Utsumi, “Stacked centrifugal microfluidic device with three-dimensional microchannel networks and multifunctional capillary bundle structures for immunoassay,” *Sensors and Actuators, B: Chemical*, vol. 166-167, pp. 898–906, 2012.
- [34] B. S. Lee, J. N. Lee, J. M. Park, J. G. Lee, S. Kim, Y. K. Cho, and C. Ko, “A fully automated immunoassay from whole blood on a disc,” *Lab on a Chip*, vol. 9, no. 11, pp. 1548–1555, 2009.
- [35] J. Park, V. Sunkara, T. H. Kim, H. Hwang, and Y. K. Cho, “Lab-on-a-disc for fully integrated multiplex immunoassays,” *Analytical Chemistry*, vol. 84, no. 5, pp. 2133–2140, 2012.
- [36] M. Ishizawa, T. Azeta, H. Nose, Y. Ukita, and Y. Utsumi, “Three-dimensional lab-on-a-CD with enzyme-linked immunosorbent assay,” *2012 7th IEEE International Conference on Nano/Micro Engineered and Molecular Systems, NEMS 2012*, pp. 213–217, 2012.
- [37] S. Okamoto and Y. Ukita, “Automatic microfluidic enzyme-linked immunosorbent assay based on CLOCK-controlled autonomous centrifugal microfluidics,” *Sensors and Actuators, B: Chemical*, vol. 261, pp. 264–270, 2018.
- [38] T. H. G. Thio, F. Ibrahim, W. Al-Faqheri, N. Soin, M. K. Bador, and M. Madou, “Sequential push-pull pumping mechanism for washing and evacuation of an immunoassay reaction chamber on a microfluidic CD platform,” *PLoS ONE*, vol. 10, no. 4, pp. 1–17, 2015.

- [39] K. Wang, R. Liang, H. Chen, S. Lu, S. Jia, and W. Wang, “A microfluidic immunoassay system on a centrifugal platform,” *Sensors and Actuators, B: Chemical*, vol. 251, pp. 242–249, 2017.
- [40] M. M. Aeinehvand, R. F. Martins Fernandes, M. F. Jiménez Moreno, V. J. Lara Díaz, M. Madou, and S. O. Martinez-Chapa, “Aluminium valving and magneto-balloon mixing for rapid prediction of septic shock on centrifugal microfluidic platforms,” *Sensors and Actuators, B: Chemical*, vol. 276, no. August, pp. 429–436, 2018.
- [41] A. Thiha and F. Ibrahim, “A Colorimetric Enzyme-Linked Immunosorbent Assay (ELISA) Detection Platform for a Point-of-Care Dengue Detection System on a Lab-on-Compact-Disc,” *Sensors*, vol. 15, pp. 11431–11441, 2015.
- [42] M. M. Aeinehvand, L. Weber, M. Jiménez, A. Palermo, M. Bauer, F. F. Loeffler, F. Ibrahim, F. Breitling, J. Korvink, M. Madou, D. Mager, and S. O. Martínez-Chapa, “Elastic reversible valves on centrifugal microfluidic platforms,” *Lab on a Chip*, vol. 19, no. 6, pp. 1090–1100, 2019.
- [43] M. Tang, G. Wang, S. K. Kong, and H. P. Ho, “A review of biomedical centrifugal microfluidic platforms,” *Micromachines*, vol. 7, no. 2, 2016.
- [44] J. Ducrée, S. Haeberle, S. Lutz, S. Pausch, F. Von Stetten, and R. Zengerle, “The centrifugal microfluidic Bio-Disk platform,” *Journal of Micromechanics and Microengineering*, vol. 17, no. 7, 2007.
- [45] O. Strohmeier, F. V. Stetten, R. Zengerle, and N. Paust, “Centrifugal microfluidic platforms : advanced unit operations and applications,” *Chemical Society Reviews*, vol. 44, pp. 6187–6229, 2015.
- [46] R. Gorkin, J. Park, J. Siegrist, M. Amasia, B. S. Lee, J. M. Park, J. Kim, H. Kim, M. Madou, and Y. K. Cho, “Centrifugal microfluidics for biomedical applications,” *Lab on a Chip*, vol. 10, no. 14, pp. 1758–1773, 2010.
- [47] D. C. Duffy, H. L. Gillis, J. Lin, N. F. Sheppard, and G. J. Kellogg, “Microfabricated centrifugal microfluidic systems: Characterization and multiple enzymatic assays,” *Analytical Chemistry*, vol. 71, no. 20, pp. 4669–4678, 1999.
- [48] S. Smith, D. Mager, A. Perebikovskiy, E. Shamloo, D. Kinahan, R. Mishra, S. M. Torres Delgado, H. Kido, S. Saha, J. Ducrée, M. Madou, K. Land, and J. G. Korvink, “CD-based microfluidics for primary care in extreme point-of-care settings,” *Micromachines*, vol. 7, no. 2, 2016.

- [49] M. M. Aeinehvand, I. Fatimah, W. Al-Faqheri, K. Joseph, and M. J. Madou, “Recent advances in the development of micropumps, microvalves and micromixers and the integration of carbon electrodes on centrifugal microfluidic platforms,” *International Journal of Nanotechnology*, vol. 15, no. 1/2/3, pp. 53–68, 2018.
- [50] M. S. Choi and J. C. Yoo, “Automated Centrifugal-Microfluidic Platform for DNA Purification Using Laser Burst Valve and Coriolis Effect,” *Applied Biochemistry and Biotechnology*, vol. 175, no. 8, pp. 3778–3787, 2015.
- [51] M. Amasia, M. Cozzens, and M. J. Madou, “Centrifugal microfluidic platform for rapid PCR amplification using integrated thermoelectric heating and ice-valving,” *Sensors and Actuators, B: Chemical*, vol. 161, no. 1, pp. 1191–1197, 2012.
- [52] M. M. Aeinehvand, P. Magaña, M. S. Aeinehvand, O. Aguilar, M. J. Madou, and S. O. Martinez-Chapa, “Ultra-rapid and low-cost fabrication of centrifugal microfluidic platforms with active mechanical valves,” *RSC Advances*, vol. 7, no. 87, pp. 55400–55407, 2017.
- [53] Z. Cai, J. Xiang, and W. Wang, “A pinch-valve for centrifugal microfluidic platforms and its application in sequential valving operation and plasma extraction,” *Sensors & Actuators: B. Chemical*, vol. 221, pp. 257–264, 2015.
- [54] Z. Cai, J. Xiang, H. Chen, and W. Wang, “Membrane-based valves and inward-pumping system for centrifugal microfluidic platforms,” *Sensors and Actuators, B: Chemical*, vol. 228, pp. 251–258, 2016.
- [55] M. M. Aeinehvand, F. Ibrahim, S. W. Harun, A. Kazemzadeh, H. A. Rothan, R. Yusof, and M. Madou, “Reversible thermo-pneumatic valves on centrifugal microfluidic platforms,” *Lab on a Chip*, vol. 15, no. 16, pp. 3358–3369, 2015.
- [56] M. M. Rashid, M. K. Al Mesfer, H. Maseem, and M. Danish, “Hydrogen Production by Water Electrolysis: A Review of Alkaline Water Electrolysis, PEM Water Electrolysis and High Temperature Water Electrolysis,” *International Journal of Engineering and Advanced Technology*, vol. 4, no. 3, pp. 1–13, 2015.
- [57] K. Zeng and D. Zhang, “Recent progress in alkaline water electrolysis for hydrogen production and applications,” *Progress in Energy and Combustion Science*, vol. 36, no. 3, pp. 307–326, 2010.
- [58] D. M. F. Santos, C. A. C. Sequeira, and J. L. Figueiredo, “Hydrogen production by alkaline water electrolysis,” *Quimica Nova*, vol. 36, no. 8, pp. 1176–1193, 2013.

- [59] N. Nagai, M. Takeuchi, T. Kimura, and T. Oka, “Existence of optimum space between electrodes on hydrogen production by water electrolysis,” *International Journal of Hydrogen Energy*, vol. 28, no. 1, pp. 35–41, 2003.
- [60] R. Natu, M. Islam, J. Gilmore, and R. Martinez-Duarte, “Shrinkage of SU-8 microstructures during carbonization,” *Journal of Analytical and Applied Pyrolysis*, vol. 131, no. January, pp. 17–27, 2018.
- [61] A. Mardegan, R. Kamath, S. Sharma, P. Scopece, P. Ugo, and M. Madou, “Optimization of Carbon Electrodes Derived from Epoxy-based Photoresist,” *Journal of The Electrochemical Society*, vol. 160, no. 8, pp. B132–B137, 2013.
- [62] M. Kakunuri and C. S. Sharma, “Effect of Pyrolysis Temperature on Electrochemical Performance of SU-8 Photoresist Derived Carbon Films,” *ECS Journal of Solid State Science and Technology*, vol. 6, no. 6, pp. M3001–M3006, 2016.
- [63] R. Martinez-Duarte, “SU-8 photolithography as a toolbox for carbon MEMS,” *Micromachines*, vol. 5, no. 3, pp. 766–782, 2014.
- [64] B. Pramanick, M. Vazquez-Pinon, A. Torres-Castro, S. O. Martinez-Chapaa, and M. Madou, “Effect of pyrolysis process parameters on electrical, physical, chemical and electro-chemical properties of SU-8-derived carbon structures fabricated using the C-MEMS process,” *Materials Today: Proceedings*, vol. 5, no. 3, pp. 9669–9682, 2018.
- [65] O. Pilloni, M. Madou, D. Mendoza, S. Muhl, and L. Oropeza-Ramos, “Methodology and fabrication of adherent and crack-free SU-8 Photoresist-derived Carbon MEMS on Fused Silica Transparent Substrates,” *Journal of Micromechanics and Microengineering*, vol. 29, 2019.
- [66] S. Sharma, “Glassy Carbon: A promising material for micro and nanomanufacturing,” *Materials*, vol. 11, no. 10, 2018.
- [67] J. Hofflin, S. M. Torres Delgado, F. Suarez Sandoval, J. G. Korvink, and D. Mager, “Electrifying the disk: A modular rotating platform for wireless power and data transmission for Lab on a Disk application,” *Lab on a Chip*, vol. 15, no. 12, pp. 2584–2587, 2015.
- [68] K. Joseph, F. Ibrahim, J. Cho, T. H. G. Thio, W. Al-Faqheri, and M. Madou, “Design and development of micro-power generating device for biomedical applications of lab-on-a-disc,” *PLoS ONE*, vol. 10, no. 9, 2015.

- [69] Y. Zhu, Y. Chen, X. Meng, J. Wang, Y. Lu, Y. Xu, and J. Cheng, “Comprehensive Study of the Flow Control Strategy in a Wirelessly Charged Centrifugal Microfluidic Platform with Two Rotation Axes,” *Analytical Chemistry*, vol. 89, no. 17, pp. 9315–9321, 2017.
- [70] S. M. Torres Delgado, J. G. Korvink, and D. Mager, “The eLoaD platform endows centrifugal microfluidics with on-disc power and communication,” *Biosensors and Bioelectronics*, vol. 117, pp. 464–473, 2018.
- [71] S. M. Delgado, F. S. Sandoval, J. G. Korvink, and D. Mager, “A universal and stand-alone datalogger for lab-on-a-disc applications,” *2016 IEEE Wireless Power Transfer Conference, WPTC 2016*, no. 3, pp. 2–5, 2016.
- [72] S. M. Delgado, D. J. Kinahan, F. S. Sandoval, L. A. N. Julius, N. A. Kilcawley, J. Ducrée, and D. Mager, “Fully automated chemiluminescence detection using an electrified-Lab-on-a-Disc (eLoaD) platform,” *Lab on a Chip*, vol. 16, no. 20, pp. 4002–4011, 2016.
- [73] S. M. Torres Delgado, D. J. Kinahan, L. A. Nirupa Julius, A. Mallette, D. S. Ardila, R. Mishra, C. M. Miyazaki, J. G. Korvink, J. Ducrée, and D. Mager, “Wirelessly powered and remotely controlled valve-array for highly multiplexed analytical assay automation on a centrifugal microfluidic platform,” *Biosensors and Bioelectronics*, vol. 109, pp. 214–223, 2018.
- [74] M. Uttamchandani and S. Yao, “Peptide Microarrays: Next Generation Biochips for Detection, Diagnostics and High-Throughput Screening,” *Current Pharmaceutical Design*, vol. 14, no. 24, pp. 2428–2438, 2008.
- [75] F. F. Loeffler, T. C. Foertsch, R. Popov, D. S. Mattes, M. Schlageter, M. Sedlmayr, B. Ridder, F. X. Dang, C. Von Bojničić-Kninski, L. K. Weber, A. Fischer, J. Greifenstein, V. Bykovskaya, I. Buliev, F. R. Bischoff, L. Hahn, M. A. Meier, S. Bräse, A. K. Powell, T. S. Balaban, F. Breitling, and A. Nesterov-Mueller, “High-flexibility combinatorial peptide synthesis with laser-based transfer of monomers in solid matrix material,” *Nature Communications*, vol. 7, no. May, pp. 1–9, 2016.
- [76] S. Aydin, “A short history, principles, and types of ELISA, and our laboratory experience with peptide/protein analyses using ELISA,” *Peptides*, vol. 72, pp. 4–15, 2015.
- [77] V. Stadler, T. Felgenhauer, M. Beyer, S. Fernandez, K. Leibe, S. Güttler, M. Gröning, K. König, G. Torralba, M. Hausmann, V. Lindenstruth, A. Nesterov,

- I. Block, R. Pipkorn, A. Poustka, F. R. Bischoff, and F. Breitling, “Combinatorial synthesis of peptide arrays with a laser printer,” *Angewandte Chemie - International Edition*, vol. 47, no. 37, pp. 7132–7135, 2008.
- [78] T. H. G. Thio, F. Ibrahim, W. Al-Faqheri, J. Moebius, N. S. Khalid, N. Soin, M. K. B. A. Kahar, and M. Madou, “Push pull microfluidics on a multi-level 3D CD,” *Lab on a Chip*, vol. 13, no. 16, pp. 3199–3209, 2013.

Appendix A: Design of electrical circuit and initial CD

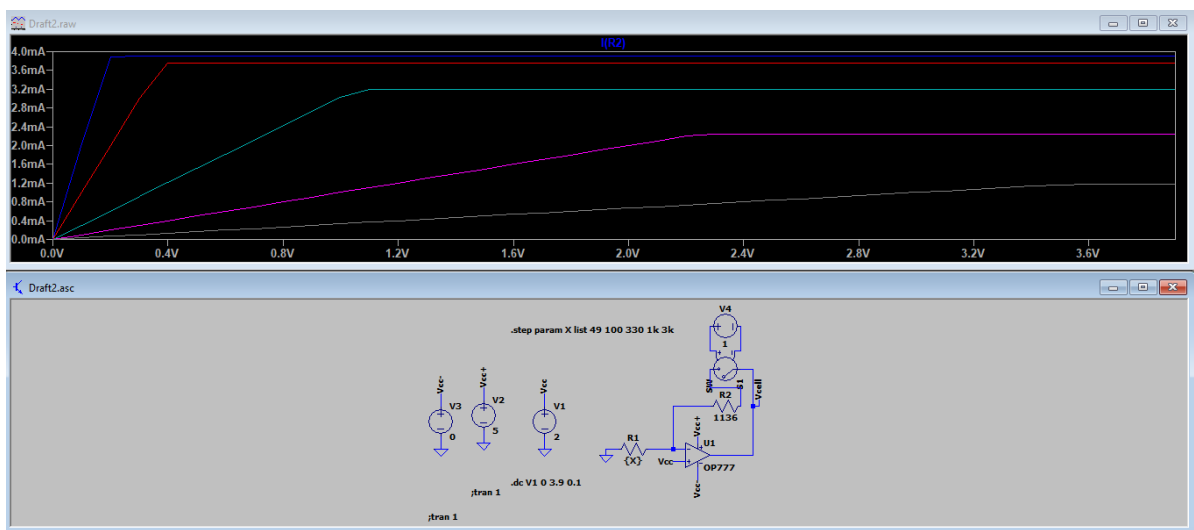


Figure 7.1: *LTSpice simulation about the current output using OP777.*

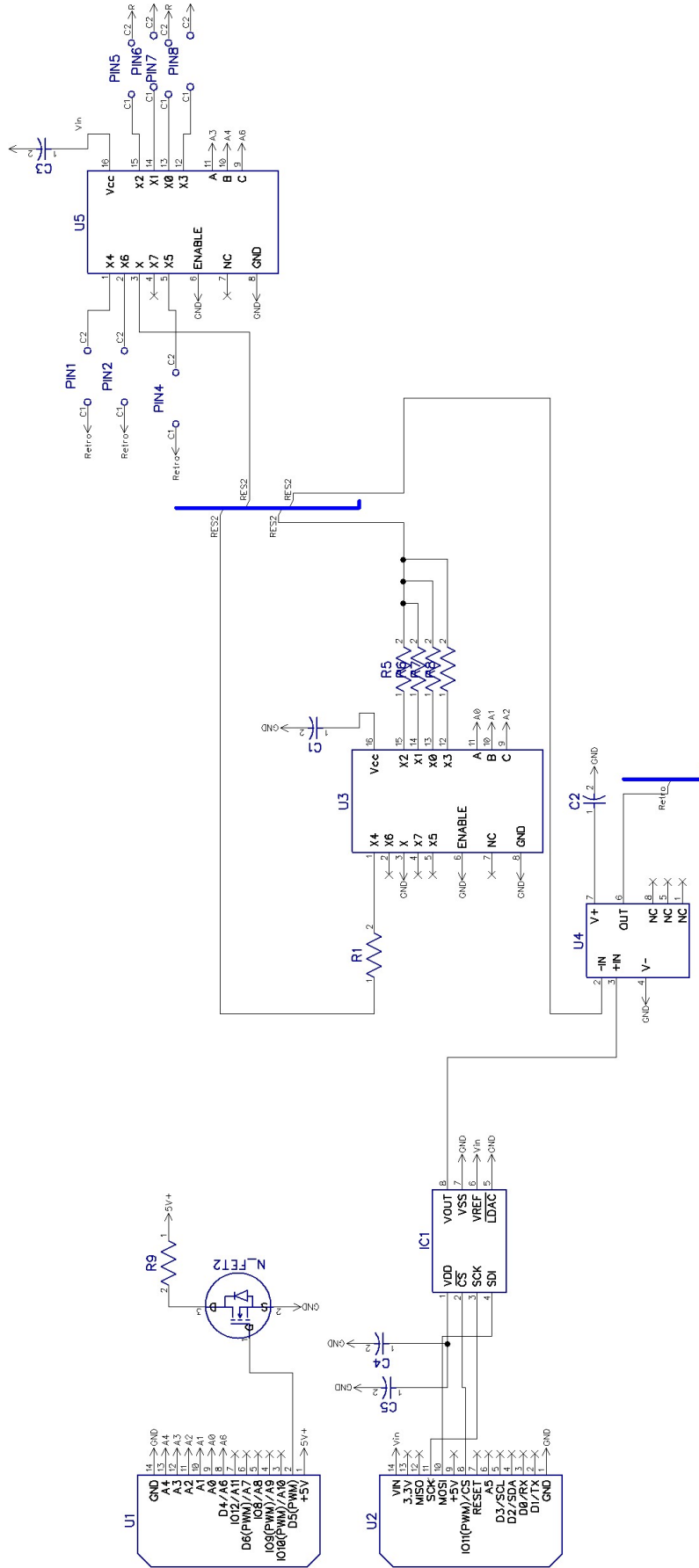


Figure 7.2: Circuit diagram of the PCB board used for immunoassay test (Phase 2 CD). This circuit enables the modulation of current to supply to the electrolysis pumps and the actuation of the electrical resistor for the RTPV.

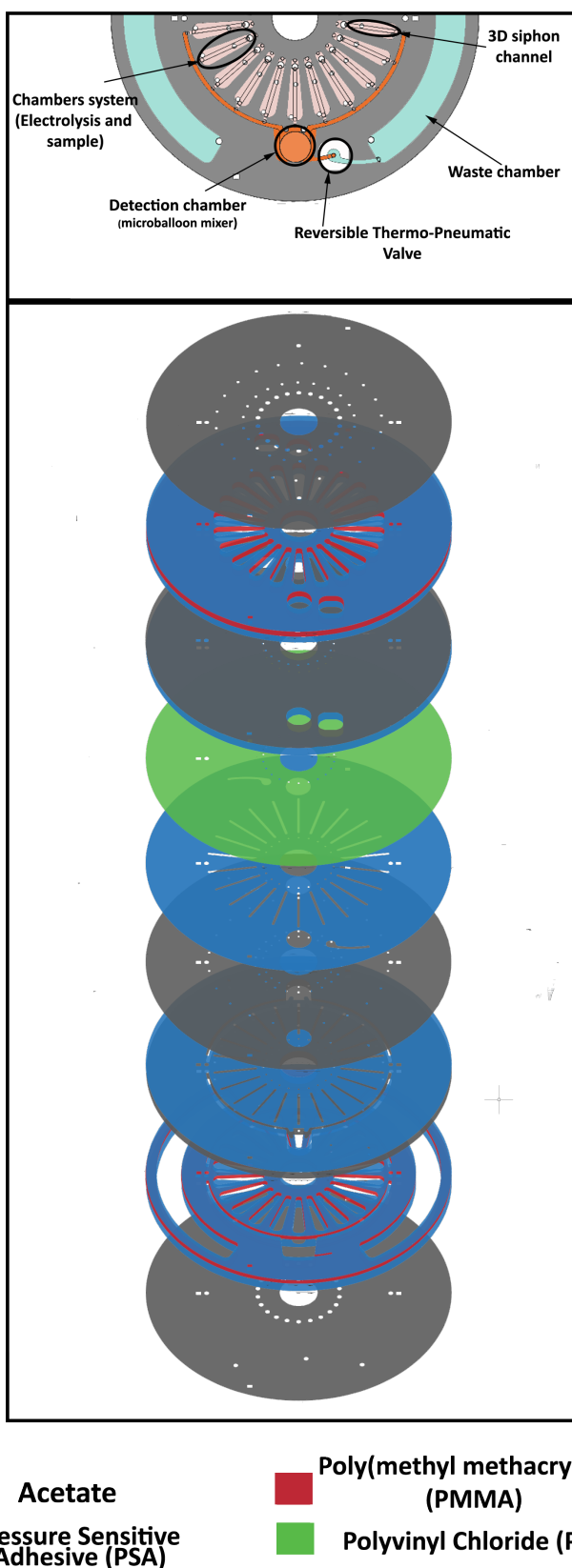


Figure 7.3: *Disc design components for preliminary adaption of immunoassay protocol. This design considers the use of electrolysis pumps and RTPV valve for liquid control.*

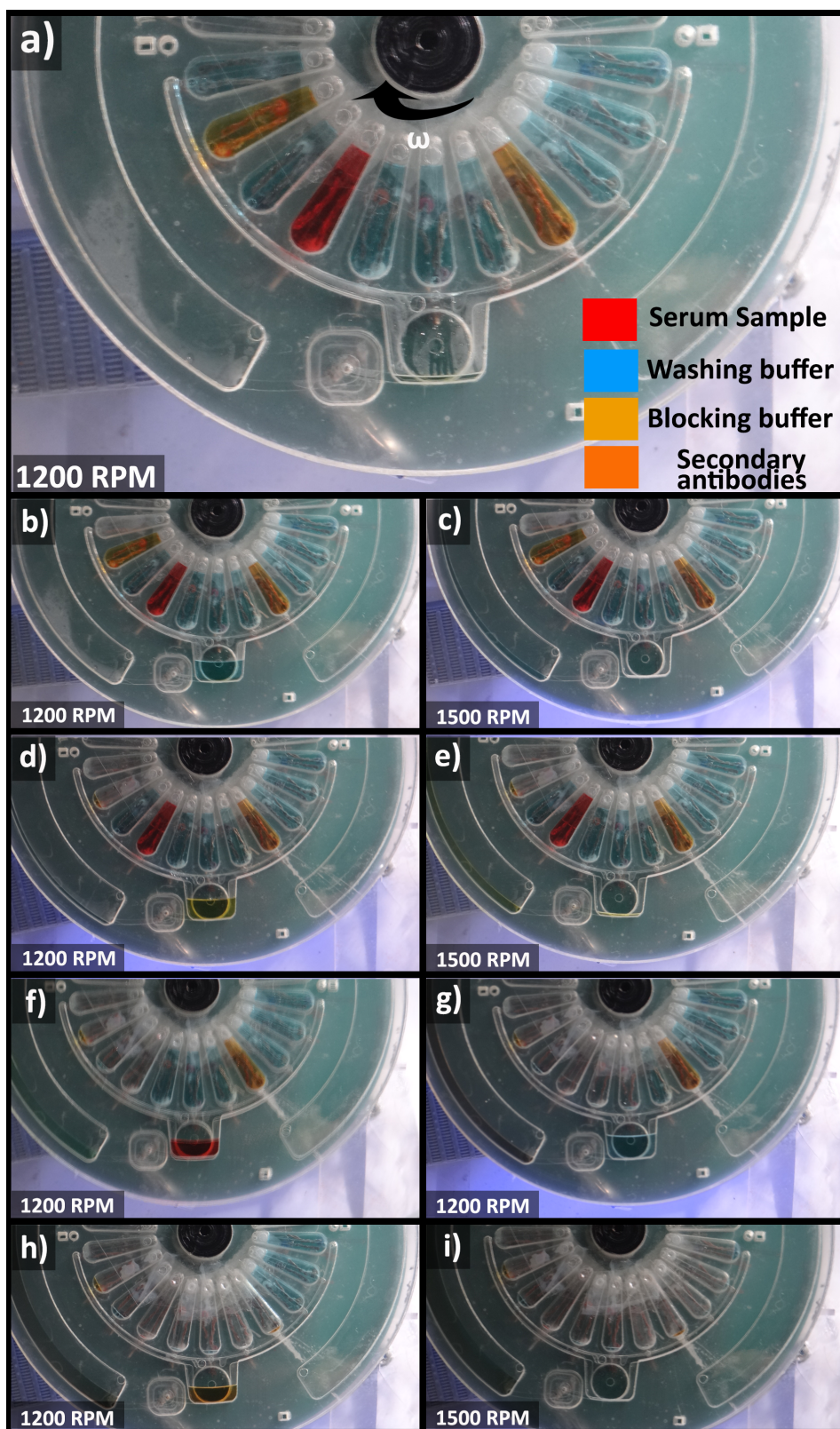


Figure 7.4: *Photos showing the operation of the initial CD design for immunoassay.*

Appendix B:Source codes



Figure 7.5: *Screenshot of block programming for android application used on Phase 2 CD on MIT Appinventor webpage.*

Arduino code for eLoaD-PCB used on immunoassay (Phase 2)

```
#include <SoftwareSerial.h>
#include <SPI.h>

String collector="";
int receivedTemp=0;
int Pump=0;
byte VoltageDAC2=0b00110000;
byte VoltageDAC1=0b10100100;
byte VoltageDAC0=0b00000000;

const int slaveSelectPin=11;
```

```
void setup()
{

SPI.begin();
SPI.setBitOrder(MSBFIRST);

    pinMode(slaveSelectPin , OUTPUT);
    pinMode(A0,OUTPUT);
    pinMode(A1,OUTPUT);
    pinMode(A2,OUTPUT);
    pinMode(A3,OUTPUT);
    pinMode(A4,OUTPUT);
    pinMode(A6,OUTPUT);
    pinMode(5,OUTPUT);

    digitalWrite(A0,LOW);
    digitalWrite(A1,HIGH); //Pins to select the input on the switch related
    digitalWrite(A2,LOW);

    digitalWrite(A3,HIGH);
    digitalWrite(A4,HIGH); //Pins to select the Pump to reconnect. It will st
    digitalWrite(A6,HIGH);

    digitalWrite(5,HIGH);

    digitalWrite(slaveSelectPin ,HIGH);

    digitalWrite(slaveSelectPin ,LOW);
    SPI.transfer(VoltageDAC2);
    SPI.transfer(VoltageDAC1);
    digitalWrite(slaveSelectPin ,HIGH);

    Serial.begin(9600); //It will be deleted in the final version of the c
    Serial1.begin(9600);
}
```

```
void loop ()
{
  while (Serial1.available()>0)
  {
    collector = Serial1.readString ();

    if (collector.indexOf("v")>=0)
    {
      collector.remove(0,1);
      receivedTemp=collector.toInt ();
    }

    if (collector.indexOf("p")>=0)
    {
      collector.remove(0,1);
      Pump=collector.toInt ();
    }
    collector="";
  }

  if (receivedTemp==1)
  {
    digitalWrite(5,LOW);
    receivedTemp=0;
  }
  if (receivedTemp==2)
  {
    digitalWrite(5,HIGH);
    receivedTemp=0;
  }

  if (Pump==1)
  {
    digitalWrite(A3,LOW);
    digitalWrite(A4,LOW); // Pins to select the Pump to reconnect. It w
    digitalWrite(A6,LOW);
```

```
Pump=0;
}
if (Pump==2)
{
digitalWrite(A3,HIGH);
digitalWrite(A4,LOW);// Pins to select the Pump to reconnect. It w
digitalWrite(A6,LOW);
Pump=0;
}
if (Pump==3)
{
digitalWrite(A3,LOW);
digitalWrite(A4,HIGH);// Pins to select the Pump to reconnect. It
digitalWrite(A6,LOW);
Pump=0;
}
if (Pump==4)
{
digitalWrite(A3,HIGH);
digitalWrite(A4,HIGH);// Pins to select the Pump to reconnect. It
digitalWrite(A6,LOW);
Pump=0;
}
if (Pump==5)
{
digitalWrite(A3,LOW);
digitalWrite(A4,LOW);// Pins to select the Pump to reconnect. It w
digitalWrite(A6,HIGH);
Pump=0;
}
if (Pump==6)
{
digitalWrite(A3,HIGH);
digitalWrite(A4,LOW);// Pins to select the Pump to reconnect. It w
digitalWrite(A6,HIGH);
Pump=0;
}
```



```
if (Pump==7)
{
digitalWrite(A3,LOW);
digitalWrite(A4,HIGH);// Pins to select the Pump to reconnect. It
digitalWrite(A6,HIGH);
Pump=0;
}
if (Pump==8)
{
digitalWrite(A3,HIGH);
digitalWrite(A4,HIGH);// Pins to select the Pump to reconnect. It
digitalWrite(A6,HIGH);
Pump=0;
}
```

Matlab code to analyze flow rate on videos (Phase 1)

```
video=VideoReader('C:\Users\81583\Google_Drive\VIDEOS_FAB\DISCO_3\Fabia
FR=video.FrameRate;
```

```
for img = 1:video.NumberOfFrames
    filename=sprintf('Frame_%d.jpg',img);
    frame=read(video,img);
    imwrite(frame,filename);
end
```

```
a=dir('C:\Users\81583\Documents\Frames');
out=size(a,1);
namefile='Frame_%d.jpg';
sec=1;
cont=1;
```

```
for i=2781:out
    if sec==10*FR
        sec=1;
    end
```

```
str=sprintf(namefile,i);
rgbImage = imread(str);
greenChannel = rgbImage(:,:,2);
allBlack = zeros(size(rgbImage, 1), size(rgbImage, 2), 'uint8');
just_green = cat(3, allBlack, greenChannel, allBlack);
```

```
if sec==1
imshow(just_green);
[cx,cy,x,xi,yi]= improfile(10000);
sec=sec+1;
elseif sec>1
x= improfile(just_green,xi,yi,10000);
sec=sec+1;
end
```

```
FIL = [1 -0.5];
```

```
y=filter(1,FIL,x(:, :, 2));

dy=gradient(y (:));
[pks , locs]=findpeaks(dy);
dyneg=-1*dy;
[pks2 , locs2]=findpeaks(dyneg);
[start , position1]=max(pks2(1:10 ,:));
[fin , position2]=max(pks);
distance=locs(position2 ,1)-locs2(position1 ,1);
distance_mm(cont ,1)=(distance*5)/10000;
second(cont ,1)=i/FR;
cont=cont+1;
end

distance_mm (: ,2)=second (: ,1);
z=1;
for i=1:72
    results(i ,1)=distance_mm(z ,1);
    results(i ,2)=distance_mm(z ,2);
    z=z+200;
end
```